Pulmonary Microvasculature Mimetics for Investigating the Role of Endothelial Apicobasal Polarity in Inflammation and Sepsis

Thesis Proposal

Alec Salminen

Advisors

Prof. James McGrath
Prof. Thomas Gaborski

Committee

Prof. Lisa DeLouise
Prof. Richard Waugh
Dr. Anthony Pietropaoli

Exam Chair

Prof. Danielle Benoit

April 16, 2019

Contents

Specific Aims

Sepsis, most recently defined as a life-threatening organ dysfunction caused by a dysregulated immune response to infection, is a major cause of mortality in the United States and worldwide. Signature features of sepsis pathophysiology include microvascular hyper-permeability, neutropenia, and neutrophilia, ultimately leading to systemic inflammation, decreased organ function, and death. In the lungs, these clinical symptoms of sepsis may lead to the development of acute respiratory distress syndrome (ARDS). While targeting the host immune response has shown promise in the clinic for a variety of diseases, pharmaceutical development for sepsis, a disease directly influenced by the immune system, has been largely unsuccessful. These shortcomings are partly due to difficulties involved in balancing remedial anti-inflammation with pathological immunosuppression in a patient population plagued by a malfunctioning immune system. Thus, this thesis will develop an *in vitro* platform to enable investigation of the innate immune response to local infections versus sepsis, and to ultimately guide the elucidation of novel sepsis therapeutic targets early in the drug development pipeline. Our platform - the microfluidic silicon nanomembrane-enabled pulmonary vascular barrier (µSiM-PVB) - will feature human pulmonary microvascular endothelial cells (EC) grown on a highly permeable, transparent, ultrathin membrane that separates luminal (blood side) and abluminal (basement membrane side) microfluidic compartments, allowing us to systematically study sepsis at the lab bench.

Aim 1: Develop a facile microvasculature mimetic to quantify endothelial small molecule and neutrophil permeability in the presence of physiological shear. Recently, our lab has introduced a nanomembrane-enabled microvascular mimetic (MVM) platform for *in vitro* study of the endothelium. This platform, however, is complex to build and often challenging to use. Thus, in this aim, we seek to advance the MVM platform in ways that will make the µSiM-PVB (Aims 2 and 3) a ready-to-use discovery platform. Specifically, we propose to achieve: 1) a membrane-based solution to the problem of EC loss on microporous membranes under physiological shear; 2) a high-throughput manufacturing solution; and 3) methodology for the *in situ* quantification of permeability by the diffusion of fluorescence dye. *Success Metrics*: Highly manufacturable devices that enable: 1) sustained EC culture under 4.5 dyn/cm^2 shear stress for 24 hours; 2) permeability measurements by fluorophore conjugated dextran passage that agree with conventional Transwell™ assays; 3) observable transmigration of leukocytes past live human ECs.

Aim 2: Elucidate the effects of polarized cytokine and endotoxin delivery on neutrophil dynamics and endothelial cell biology. Vascular ECs exhibit defined luminal and abluminal sides *in vivo*. This apicobasal polarity may be key to understanding the difference in vascular barrier responses to early stage infections versus the late stage systemic 'cytokine storm' observed in sepsis. Specifically, we hypothesize that neutrophil dynamics on ECs will be sensitive to human-derived cytokines and bacteria-derived endotoxins in a polarized manor. We will test this hypothesis in our µSiM-PVB by simultaneously quantifying endothelial permeability and neutrophil trafficking in response to luminal or abluminal TNF-α and lipopolysaccharide (LPS). Permeability measurements will be calculated by transendothelial diffusion of dextran as in Aim 1. Neutrophil trafficking will be quantified post-experiment in an automated fashion and correlated with endothelium permeability.

Aim 3: Demonstrate the polarized dependence of S1P in regulating pulmonary vasculature permeability and neutrophil dynamics following septic insult *in vitro*. Sphingosine-1-phaspahte (S1P) has been discovered to play a paradoxical role in the balance of endothelium permeability and leukocyte extravasation. Furthermore, its receptors (SIPR1-5) are differentially expressed on apical and basal surfaces of ECs. We hypothesize that S1P will be barrier protective when applied abluminally and barrier disruptive when applied luminally. The µSiM-PVB will be used to investigate polarized effects of S1P on neutrophil extravasation and endothelial permeability following barrier disruption via exposure to clinical septic serum. Effects will be quantified over a range of sepsis severities as defined by patient sequential organ failure assessment (SOFA) score at the time of blood draw. We expect to observe increased extravasation and permeability at all levels of sepsis severities, that is recovered with the abluminal addition of S1P.

Significance

Sepsis is a maladaptive immune response to infection[1] that affects an estimated 750,000 patients in the US every year.[2] From initial pathogen exposure to multiorgan failure (MOF), sepsis pathophysiology is defined by a complex cytokine 'storm' in the blood, leading to systemic microvascular permeability, dysregulated neutrophil response, and ultimately fatal organ dysfunction.[3-5] Currently, there are no approved pharmaceuticals for sepsis treatment and the current standard of care involves patient stabilization via auxiliary support and fluid perfusion.[3,6,7] Due to these clinical challenges, 15 – 25% of all sepsis cases do not resolve, and patients die of MOF.[8] Part of the challenge in developing therapies for sepsis is the lack of experimental models that allow high-throughput and systematic deconstruction of molecular mediators. This thesis will directly address this need by developing a facile, bench top system to test the impact of clinical septic plasma samples on microvascular permeability and neutrophil trafficking. Furthermore, targeting the immune response in sepsis requires extreme caution, as immunosuppression can lead to sever clinical complications in an already immune compromised patient population.[6,9] We propose to shift the therapeutic development approach to an *in vitro* platform that employs human cells and patient serum to elucidate potential pharmaceutical targets in a case-specific manner. Importantly, the confined geometries of our μSiM-PVB allows us to effectively evaluate patient samples using just 1-2 μL of serum, reducing the need for large blood collections and lowering the cost of experiments.

This work will specifically focus on the effects of sepsis on lung health. Sepsis is the number one risk factor for acute respiratory distress syndrome (ARDS), a condition marked by acute lung injury and impaired oxygenation of the blood.[10] During every cardiac cycle, the entire volume of blood passes through the lung capillaries. In sepsis, circulating inflammatory cytokines (e.g. TNF-α) can stimulate increased endothelial permeability and abnormal leukocyte extravasation or sequestration at the lung capillary bed, resulting in pulmonary edema and in some cases ARDS.[11-13] The development of pulmonary vascular hyper-permeability and ARDS is a feared complication that raises the risk of death or other adverse outcomes in patients with sepsis. Recent studies have shown that serum S1P levels are significantly correlated with the onset and progression of sepsis and ARDS.[14-16] Extensive characterization of S1P and its role in the innate and adaptive immune responses suggests that intravenous delivery of S1P would have systemic, non-specific effects, resulting in 'off-target' complications.[17,18] Given this consensus, we propose to alter the therapeutic approach by delivering S1P (or its analogs) through the abluminal interface of the endothelium, effectively isolating the barrier protective effects of the lipid. In all, this work will demonstrate the potential of novel microfluidic technology in elucidating and testing sepsis pharmaceuticals.

Innovation

The key innovation in this proposal lies in our use of ultrathin porous silicon membranes (nanomembranes) to create a facile microfluidic platform for the study of small molecule and leukocyte permeability through human pulmonary microvascular ECs. Silicon nanomembranes are free-standing, highly porous membranes developed at the University of Rochester over the last decade. They have a thickness similar to the basement membranes of tissue (50 nm – 400 nm), pore sizes that can be tuned from 30 nm and 3 μm, and porosities as high as 40%.[19] These features gives nanomembranes a diffusive permeability to small molecules shown to be orders of magnitude higher than track-etched membranes used in conventional Transwell™ devices. Recently, silicon nanomembranes have enabled the development of human blood-brain-barrier (BBB) models at the lab bench, permitting leukocyte tracking experiments previously not possible with commercially available filters.[20] In this work, we have discovered a unique protocol in which we etch micropores directly into the highly permeable nanoporous material, providing a never before achieved dual-scale membrane, with uniform permeability to small molecules and egress ports for neutrophil transmigration (**Figure 1**). Nanomembranes give glass-like image quality in both transmitted and fluorescence microscopy,[21] allowing use of inverted microscopes and phase

contrast imaging to observe the complex dynamics of neutrophils on a live human barrier model. Finally, the silicon 'chip' format enables direct integration of these nanomembranes with layer-by-layer construction typically used to fabricate microfluidic devices.[22]

Our device (µSiM-PVB) will include integrated microfluidics capable of generating flow in the apical chamber for: 1) shear-induced enhancement of vasculature barriers,[23,24] and 2) introduction of neutrophils under flow.[25] The optical quality of these devices will be compatible with high resolution phase microscopy to enable live imaging of all steps in the neutrophil transmigration program: rolling, luminal crawling, firm adhesion, diapedesis, and abluminal migration. At the same time, our µSiM-PVB will be compatible with fluorescent microscopy techniques[26] used to measure barrier permeability by monitoring the diffusion of small molecules across the monolayer into the periphery of the basolateral channel. This novel assay will allow for continuous monitoring of system permeability without disturbing the delicate biological microenvironment.

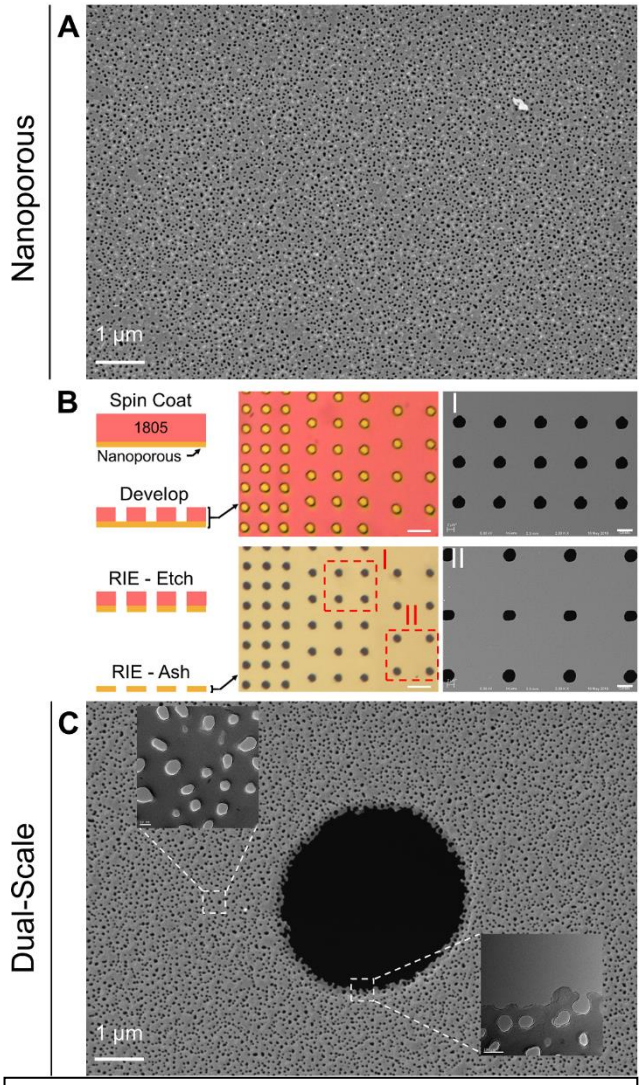

Figure 1. Fabrication of dual-scale membranes from native nanoporous silicon nitride. Nanoporous membranes (A) are lithographically fabricated and etched in the cleanroom (B). Resulting dual-scale membranes (C) contain 3 µm pores etched directly into a highly porous background. (Coat/Etch scale = 10 µm; I,II scale = 4 µm))

Having achieved the first shear influenced pulmonary vasculature mimetic compatible with live cell imaging, we will be able to perform novel studies on the role of endothelial apicobasal polarity[27-31] in regulating the innate immune response to systemic inflammation. The ability to simultaneously monitor neutrophil diapedesis and small molecule diffusion in a two-chamber living system will allow us to look for difference in the vascular response between inflammatory messages that originate in tissue versus those carried by blood; filling a key gap in knowledge necessary to advance pharmaceutical development for systemic inflammation. Only a system that can simultaneously measure vascular permeability to both leukocytes and small molecules can address these questions. To this end, highly permeable, transparent membranes, like those proposed here in, are critical characteristics of the necessary cell culture substrate.

Advancing our understanding of the role of EC apicobasal polarity in sepsis and local inflammation will have an important impact in both the critical care community and the field of EC biology. Previous sepsis therapeutics have failed to account for this area of knowledge, leading to largely disappointing clinical outcomes.[6,32-34] In close collaboration with the pulmonary and critical care team at Strong Memorial Hospital at the University of Rochester, we will be taking a translational approach to understand and address these highly relevant concerns. In utilizing serum samples from clinical sepsis cases, we will lay the foundation for the use of the µSiM-PVB as a diagnostic tool, as well as a means of exploring patient group specific drug development.

Approach

The overall goal of this project is to design a facile microfluidic system to study sepsis at the lab bench. Our guiding hypothesis is that EC apicobasal polarity regulates sepsis advancement and can inform novel therapeutic development. The first aim of this proposal is to develop and test a microphysiological vasculature mimetic with fully integrated microfluidics. Traditional Transwell™ inserts provide arrayed platforms to study cell monolayer permeability, however, poor optical properties and lack of physiological shear stress diminish the relevance of the experiments performed. A system capable of sustaining physiological levels of shear stress (~4.5 dyn/cm^2)[35] across endothelial barriers grown on highly permeable substrates is key in progressing sepsis research *in vitro*.[23] The second aim of this proposal will employ polarized delivery of inflammatory cytokines and pathogen associated molecular patterns (PAMPs) to mimic both the primary infection stage and systemic inflammatory response stage of sepsis. Neutrophil trafficking observed in these signaling scenarios will reveal the distinguishing characteristics of the phasic response. The third aim will explore the function of S1P as a polarized regulator of neutrophil extravasation and widespread vasculature permeability. This final aim will also demonstrate the potential of our vasculature mimetic for use in pharmaceutical development.

Aim 1: Develop a facile microvasculature mimetic to quantify endothelial small molecule and neutrophil permeability in the presence of physiological shear.

Rational: This aim will focus on the development of a facile microfluidic system with potential for controlled sepsis modeling and pharmaceutical development. The objective of this aim is to integrate ultrathin silicon membranes into a microfluidic system and demonstrate high content microscopy, *in situ* permeability, and high-volume manufacturing potential. To accomplish the objectives of this aim, we will test the working hypothesis that continuously permeable, nano- and micro-porous membranes can be engineered to sustain cell culture under shear while facilitating the transendothelial flux of neutrophils (through micropores) and small molecules (through nanopores). Novel cleanroom techniques with quick design iteration potential can be exploited to pinpoint the optimal membrane solution for our system. Development of a system with the aforementioned capabilities is critical when studying sepsis. The visual ques in sepsis are often underutilized in research due to imaging limitations in conventional experimental setups, both *in vivo* and *in vitro*. Our highly transparent system will provide a means of observing the maladaptive immune response to septic insult on a human PVB in real time. We expect to complete this aim with the ability to manufacture silicon membrane-based vasculature mimetics with high resolution imaging potential and sustain cell culture under physiological shear stress.

Task 1.1: Develop a membrane-based solution to the problem of shear-induced endothelial cell loss on microporous membranes. Previously our lab has developed microporous silicon dioxide (SiO_2) membranes (pore sizes ranging from 0.5 to 3 µm) for use in cell culture systems.[21,36] While these membranes provide cell biocompatibility and optical transparency, preliminary studies showed a dramatic loss of EC adhesion when cultured in a flow based system.[20,37] Paradoxically, when micropore density is decreased to the point of sustained EC adhesion, the non-continuous permeability of the substrate becomes unphysiological when compared to the proteinases vascular basement membrane.[38] On the other hand, nanoporous silicon nitride membranes[39,40] (NPN; pore sizes ranging from 10 to 100 nm) sustain EC adhesion at similar shear stress levels while maintaining continuous permeability, but lack leukocyte transmigration routes.[41] In this task, we will modify existing NPN membranes with pores large and dense enough to facilitate complete neutrophil egress, while still permitting physiological shear priming of the EC monolayer, effectively developing the first dual-scale membrane for cell culture. In the cleanroom, ultrathin (100 nm) NPN membranes (SiMPore Inc., West Henrietta, NY) will be individually coated with a 500 nm uniform coating of Shipley 1805 positive photoresist (MicroChem Corp., Westborough, MA) using manufacturer protocols. Micropore patterns illustrated in CleWin5 software will be transferred into the photoresist using a high-resolution laser writer system (MICROTECH, Palermo,

Italy). UV exposed regions will be washed away with resist developer Microposit MF-319, leaving a micropore template directly atop the ultrathin NPN membrane surface. Templated membranes will be transferred to a reactive ion etcher (RIE) system (South Bay Technology Inc., San Clemente, CA), where unprotected silicon nitride will be selectively etched away using a standard three-gas silicon etch recipe (15 SCCM O2, 10 SCCM CHF3, 30 SCCM SF6, 200 s, 30-50 mTorr, 100 W). A subsequent oxygen plasma ash step in the RIE (55 SCCM O2, 15 min, 200 mTorr, 100 W) will be used to selectively remove the remaining photoresist while allowing for batch processing of templated membranes. Enabled by the high-flexibility and low-cost of this membrane design process, an array of 3 μm pore densities (27777, 12345, 6944, 4444, 3086, 2267, 1736, and 1371 pores/mm^2) will be probed for sustained human umbilical vein endothelial cell (HUVEC) adhesion under physiological shear stress levels (4.5 dyn/cm^2). Micropore densities permitting shear priming of a HUVEC monolayer will be selected for future experimentation.

Progress: We have successfully fabricated dual-scale (nano- and micro-porous) membranes through the lithographic addition of micropores on existing NPN membranes (**Figure 1**). Dual-scale membranes were tested for biocompatibility and for their ability to permit neutrophil egress under an fMLP gradient (**Figure 2**). Membranes fabricated with an array of micropore densities elucidated a maximum pore density (6944 pores/mm^2) above which dramatic cell loss was observed under physiological shear stress (**Figure 3**). The addition of an extracellular matrix to the abluminal side of the dual-scale membrane rescued HUVEC adherence on all micropore densities (**Supplemental Figure S1**). While membrane fabrication is relatively quick in small batches (< 2 h for ~10 membranes), future work will explore the ability to fabricate these membranes on a wafer scale (~400 – 500 membranes). This work was been published in the journal, SMALL (Appendix).[38]

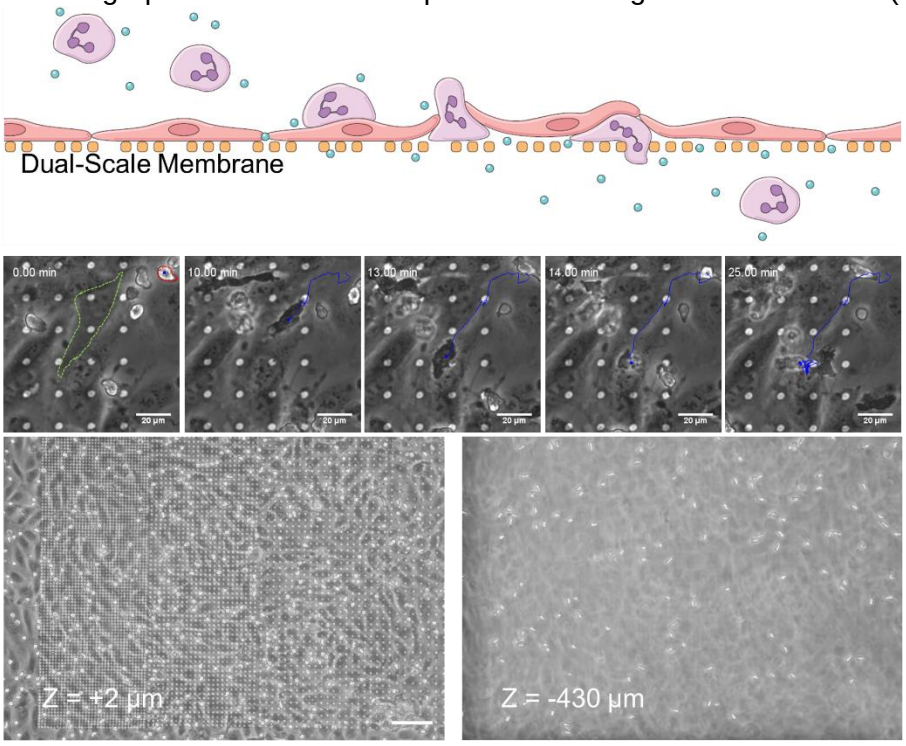

Figure 2. Dual-scale membranes support human endothelial cell culture and complete neutrophil extravasation. HUVECs seeded on dual-scale membranes were perfused with human neutrophils. Abluminally perfused chemoattractant, fMLP, drives neutrophil migration through the endothelial cell layer into the bottom channel, eventually ending up on the underlying coverslip. (Time lapse scale = 20 μm; Z-stack scale = 200 μm)

Task 1.2: Explore high-throughput manufacturing for the development of a facile microvascular mimetic system. We have previously developed custom microvascular mimetics (MVM) featuring ultrathin silicon membranes.[42] A major rate limiting step in our ability to utilize these vasculature mimetics for basic science exploration is the heavy burden of in-lab device fabrication. The current fabrication technique involves a layer-by-layer assembly that requires significant time allocation (~30 devices per month). When higher experimental replicates are desired, this low-throughput device fabrication can extend experimentation times significantly. Working with an experienced microfluidic company (Aline Inc., Rancho Dominguez, CA), we will design, test, and fabricate a fully integrated MVM platform for increased

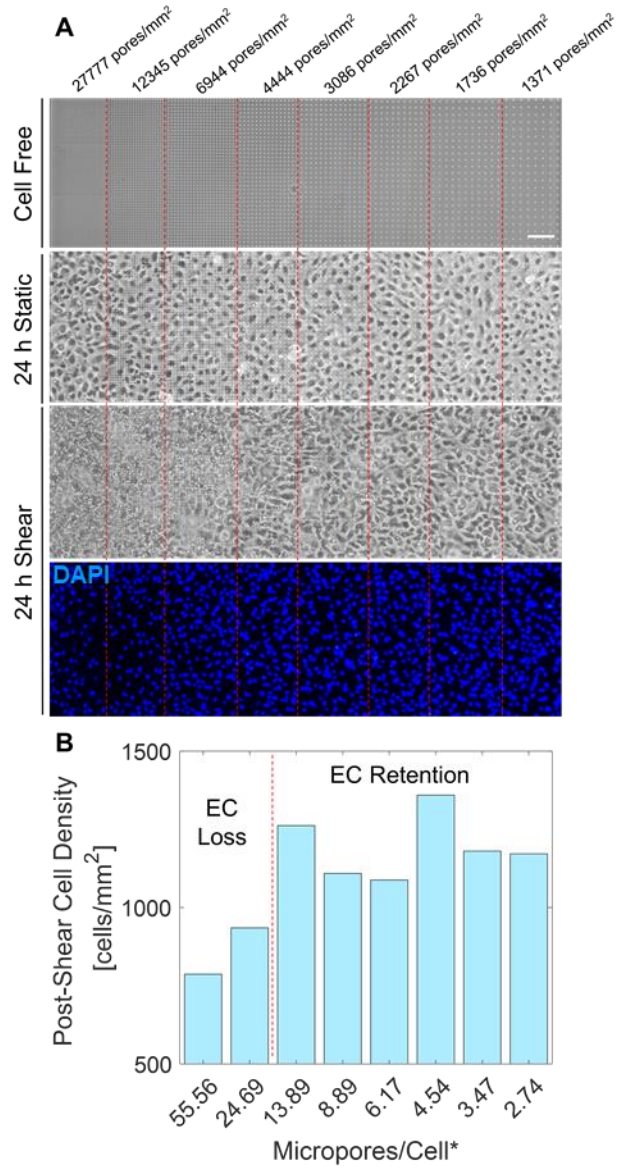

Figure 3. High micropore densities lead to endothelial cell loss under physiological shear. HUVECs seeded on gradient dual-scale membranes (A) begin to detach under 4.5 dyn/cm^2 shear once micropore density reaches > 13.89 pores/cell (B). (Scale = 100 µm)

experimental throughput. Precision laser cut acrylic, PET and COP layers bonded with pressure sensitive adhesive (PSA) will form the microfluidic unit, within which the silicon membrane will sit. The use of a laser cutter system will allow for high-throughput device fabrication (~300 devices per week). An optical layer constructed of thin COP (50 µm) will allow for a reduced optical working distance, thus permitting high resolution microscopy. Devices will be tested for biocompatibility and undesired leaking. Human pulmonary microvascular endothelial cells (HPMECs; Promo Cell, Heidelberg, Germany) will be seeded in place of HUVECs to finalize the µSiM-PVB platform.

Progress: In collaboration with Professor Edward Schwarz in the Center for Musculoskeletal Research at the University of Rochester and Aline Inc., we have designed and executed a high-throughput device fabrication protocol (**Figure 4**). This approach has been utilized for the development of the microfluidic silicon membrane canalicular array (µSiM-CA) and is outlined in a forthcoming manuscript. Early endothelial and bacterial cell culture experiments have demonstrated biocompatibility (**Supplemental Figure 2**). This platform will soon be tested for its ability to facilitate leukocyte migration experiments.

Task 1.3: Develop a protocol capable of producing accurate small molecule permeability measurements *in situ*. Endothelial monolayer permeability can be assessed by the net passage of small molecule tracers (e.g. FITC conjugated dextran) over discrete time points.[43] When addressing the progressive nature of vasculature permeability as seen in sepsis, discrete measurements may not be suitable. Furthermore, current small molecule permeability assays utilize sample collection that may disturb the sensitive system being tested, potentially leading to misinterpreted results. Frequent sample collection becomes more of a burden when considering the use of a low-volume microfluidic device like ours. We hypothesize, however, that by taking advantage of the current silicon membrane format, we can physically block out-of-focus fluorescence within our system, allowing for *in situ* small molecule permeability measurements on an epifluorescence microscopy setup without disturbing the cell culture system. HUVECs will be grown within our standard microfluidic device assembly and exposed to 4.5 dyn/cm^2 for 24 h. Control devices will be incubated for 24 h without flow. Devices will be transferred to an incubated (37°C, 5% CO_2) microscope stage-top chamber on a Nikon TS100. A 40X objective will be focused beneath the silicon scaffolding layer to detect EC passage of fluorescent small molecules. FITC-Dextran (10 kDa and 70 kDa) in standard HUVEC media (MCDB-131 complete media; Vec Technologies

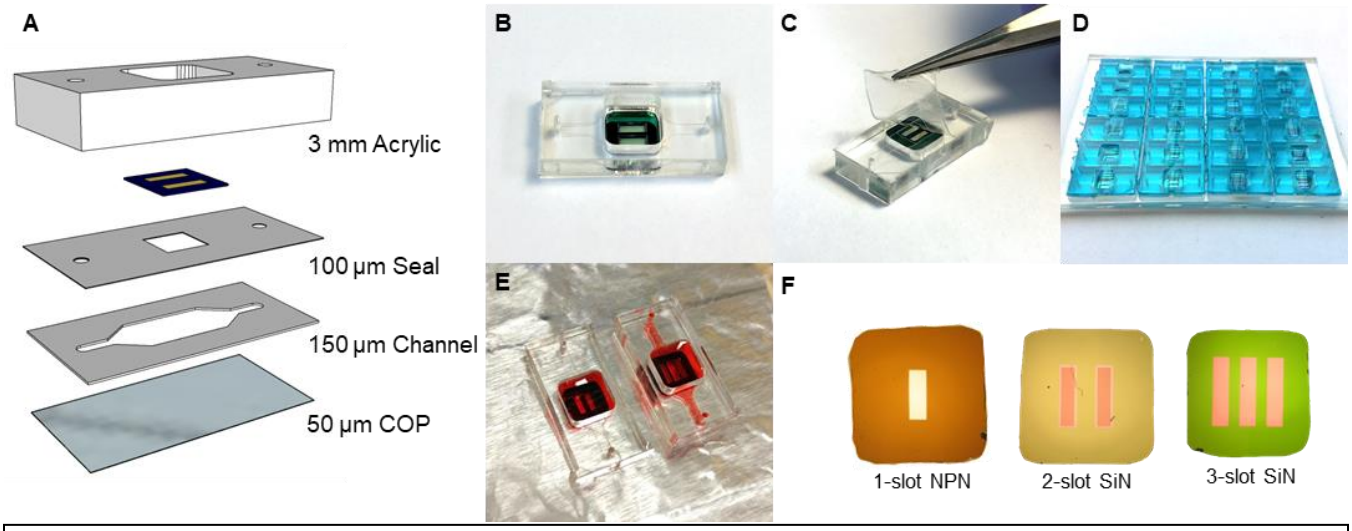

Figure 4. High-throughput device fabrication allows for 300-unit production in ~ 1 week. Devices are produced in a layer-by-layer lamination process (A), resulting in a compact unit (B) for experimentation. Removable optical layer allows for facile SEM integration (C). Devices are produced in batch (D) and retain fluidic seal (E). The fabrication process is compatible with a variety of membrane formats depending on use (F).

Inc., Rensselaer, NY) will be perfused into the luminal (top) chamber of our vasculature mimetic at a final concentration of 1 mg/ml and epifluorescence time-lapse imaging will be initiated. Human thrombin (5 U/ml; Sigma), a known EC barrier disrupter, will be used as a positive control. FITC-Dextran flux comparisons between sheared, static, and thrombin treated devices will demonstrate the sensitivity of our assay in detecting shear and chemical-influenced changes in HUVEC permeability. The diffusive behaviors seen in this experimental setup can be explained by the solution of Fick's second law in a semi-infinite medium with a constant source (Equation 1).[44]

$$C_x = C_o erfc\left(\frac{x}{2\sqrt{Dt}}\right) \quad (1)$$

Where C_x is the concentration distance, x, from the membrane center, C_o is the concentration in the top channel, D is the diffusion coefficient extracted from the data, and t is the time of experiment. When we consider Beer-Lambert law, relating absorbance to concentration, we can predict that the concentration of the fluorescence tracer is proportional to the fluorescence intensity, I, picked up by our microscope. Therefore, for experimental purposes, Equation 1 can be rewritten as Equation 2.

$$I_x = I_o erfc\left(\frac{x}{2\sqrt{Dt}}\right) \quad (2)$$

Where I_x is the fluorescence intensity distance, x, from the membrane center, and I_o is the fluorescence intensity of the input fluorophore solution. To our advantage, when I_o is divided through Equation 2, the left side of the equation ($\frac{I_x}{I_o}$) becomes unitless. In this form, we may input experimental data in place of this unitless variable and obtain a diffusion coefficient (D), predictive of system permeability. Finally, this permeability can used to solve for EC permeability (P_{EC}; Equation 3).

$$\frac{1}{P_{EC}} = \frac{x}{D} - \frac{L}{D_{dextran}} \quad (3)$$

Where x is the distance from the center of the membrane to the detector, D is the diffusion coefficient extracted from the experimental fit of Equation 2, L is the distance from the membrane edge to the detector, and $D_{dextran}$ is the diffusion coefficient for dextran 37 °C media.

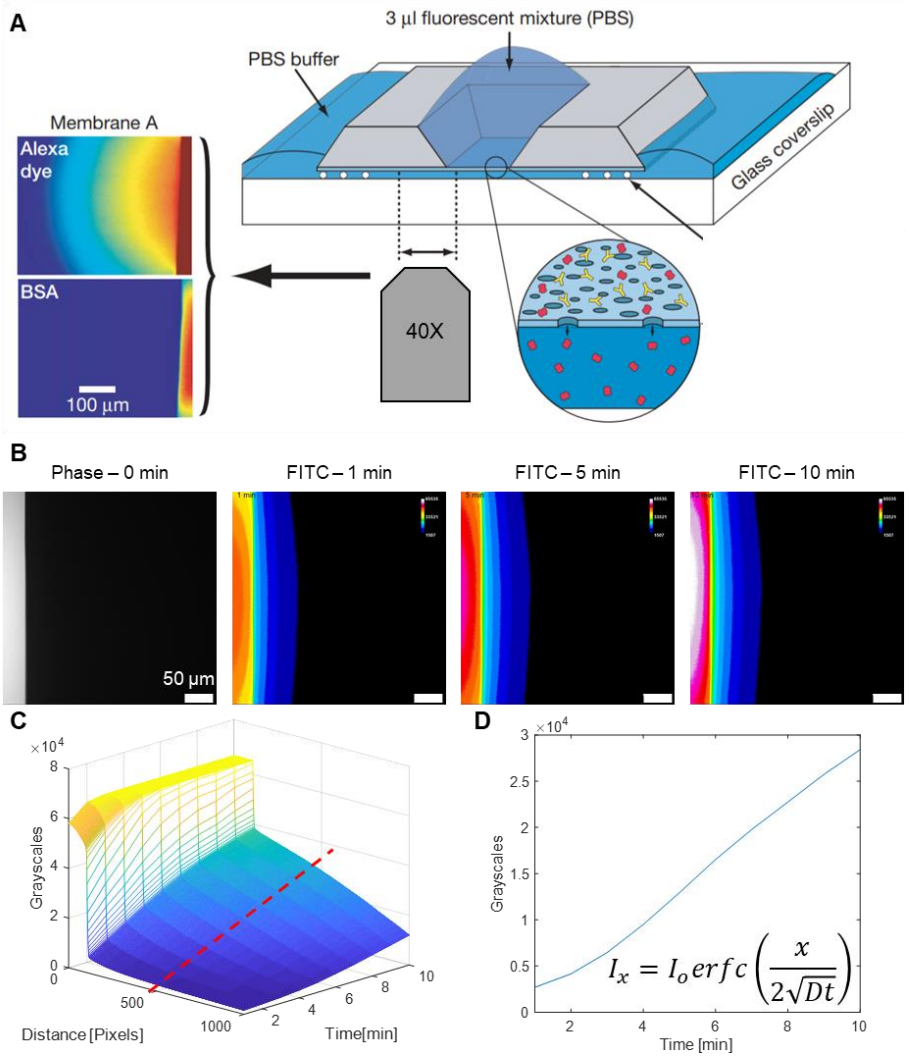

Figure 5. *In Situ* permeability measurements may be performed in a facile epifluorescence configuration. Based on a previously published assay (A [Striemer et al., Nature 2007]), FITC-dextran diffusion is monitored via 40X epifluorescence microscopy (B; Scale bars = 50 µm) in the bottom channel of the µSiM-PVB over a defined experimental time (C). Changes in fluorescence intensity across a single line (D) are influenced by device permeability as predicted by Equation 2. Background permeability can be subtracted to obtain permeability of the endothelial cell layer.

Progress: Early experiments demonstrated the utility of this assay in measuring 10 kDa FITC-dextran flux across an EC monolayer and the accompanying silicon membrane (**Figure 5**). Currently we are developing a COMSOL model for the prediction of endothelial monolayer permeability based on the progression of fluorescence intensity over time. In brief, we will use our COMSOL simulation to build a database of experimental scenarios based on variation in EC permeability values. These simulations will subsequently be analyzed for concentration progression through a point 400 µm (*x*, Equation 2) from the membrane center (50 µm off the membrane edge), and this data will be normalized to the input fluorophore concentration (C_o), effectively providing an array of $\frac{C_{50\ \mu m}}{C_0}$ values. This array can then be compared to experimental data collected in the lab (effectively $\frac{I_{50\ \mu m}}{I_o}$; **Figure 5D**) to predict the permeability of the respective EC monolayer.

Expected Outcomes

By the completion of this aim, we expect to have built and characterized a silicon membrane-based microfluidic device with the ability to sustain cell culture under physiological shear. Ultrathin silicon membranes will be selected based on promotion of cell viability and assay development as determined in **Tasks 1.1** and **1.3**. More specifically, the membrane must allow for unhindered small molecule (dextran) and neutrophil transmigration while providing sufficient surface area to sustain cell adhesion under shear stress equal to that of the post-capillary venules. Our vasculature mimetic in the proposed format will provide all the tools to assess vasculature damage and leukocyte trafficking following inflammatory stimuli, while permitting flexibility to change the cell type, and membrane format on an experimental need basis. Furthermore, a high-throughput manufacturing alternative will advance our experimental throughput, thus providing a means for sepsis exploration in subsequent aims.

Potential Problems and Future Directions
Much of the research proposed in **Aim 1** has been completed (**Task 1.1**[38]) or is in late stages (**Tasks 1.2** and **1.3**). For this reason, early problems in our experimental design have been solved. One aspect of our proposal that still needs to be addressed is our approach to high-throughput device fabrication. In its current form, these devices have solved our need for 'Transwell' like cell culture platforms, however, they do not allow for shear. To overcome this limitation, we plan to build a flow adapter around the current device design. Fabricated in collaboration with Professor Vinay Abhyankar of RIT, this adapter will allow for facile integration of the microfluidic devices into a flow cell, effectively forming a fluid sealed top channel with pump inlet and outlet connections. In order to have successfully completed fabrication of a flow cell adapter, we must achieve: 1) sustained flow through an added top channel necessary to achieve 4.5 dyn/cm^2 shear stress over 24 h, 2) reusable parts not including the replaceable cell culture device as produced by Aline Inc. and, 3) integration into a peristaltic pump circuit for recycled media flow.

Aim 2: Elucidate the effects of polarized cytokine and endotoxin delivery on neutrophil dynamics and endothelial cell biology.

Hypothesis and Rational: Sepsis can take on differing trajectories and outcomes, usually preceded by an early stage hyperinflammatory response.[3] While 15-25% of sepsis cases do not resolve past the hyperinflammatory stage and result in patient death, many patients do recover from this maladaptive immune response. Persistent immunosuppression and catabolism syndrome (PICS) is a complication for many recovered patients, leading to increased susceptibility to infection. Not surprisingly, therapies targeting the maladaptive immune response in sepsis have been pulled from clinical trials because they chronically suppress the immune system.[9,32-34,45] Advancing our understanding of the distinguishing characteristics of systemic immune responses and primary infections is necessary to develop novel sepsis therapeutics that do not exacerbate the risk for subsequent pathogen attack. We hypothesize that EC apicobasal polarity in response to inflammatory markers will dictate neutrophil dynamics and vascular damage, thus providing a means of specifically targeting the maladaptive immune response to systemic factors. Considering our ability to observe neutrophil trafficking across a highly permeable support capable of abluminal cytokine and endotoxin delivery, we believe the µSiM-PVB with the accompanying dual-scale membrane as developed in **Aim 1** is capable of permitting the outlined studies.

Task 2.1: Develop methods for the automated quantification of leukocyte dynamics within our µSiM-PVB. As mentioned, an important feature of the µSiM-PVB's silicon nitride membrane over tradition polymeric membranes is the improved imaging potential. These optical properties allow for phase time-lapse imaging, thus permitting real-time neutrophil tracking without the need for fluorescent dyes. Previous studies have demonstrated the ability to track neutrophil dynamics on glass substrates,[46,47] however, these substrates do not enable permeability or abluminal small molecule delivery experiments proposed here. Prior to execution of these studies we must explore the use of objective automated leukocyte tracking for unbiased and efficient data collection. In collaboration with Professor Douglas Kelley's lab at the University of Rochester, we will modify a previously established particle tracking algorithm[48-50] to enable leukocyte tracking from phase contrast movies. The code will exploit the distinguishable pixel intensity changes (phase white to phase dark) observed on our membranes between luminally crawling leukocytes, ECs, and abluminally crawling leukocytes, to track all phases of extravasation. Additionally, this algorithm will identify transitions in single cell pixel intensity to mark specific locations of leukocyte diapedesis. Successful adaptation of this code will enable spatial and temporal tracking of luminal and abluminal leukocyte dynamics, as well as spatial and temporal tracking of egress points.

Progress: Preliminary implementation of the code developed by the Kelley lab has shown the ability to track and mark aspects of the leukocyte extravasation cascade, including luminal crawling, transmigration, and abluminal crawling (**Figure 6**). The algorithm, however, may benefit from increased

contrast (i.e. larger pixel intensity separation) between the ECs and the neutrophils. Future work will involve improving the phase microscopy setup to better distinguish the two groups. Additionally, we will be performing a head-to-head comparison of automated to hand tracked data to establish confidence in the conclusions extracted from the algorithm.

Task 2.2: Investigate the effects of polarized cytokine and endotoxin delivery on leukocyte dynamics *in vitro*. This task will involve the first implementation of the µSiM-PVB for the study of biological phenomena. HPMECs will be seeded in the µSiM-PVB at a density equal to 40,000 cells/cm^2 to achieve a confluent monolayer after attachment. Two hours post-seeding, the µSiM-PVB will be assembled into the fluidics circuit, and HPMECs will be exposed to 4.5 dyn/cm^2 shear stress for 24 h. Shear primed endothelial cells will then be statically incubated with human recombinant TNF-α (20 ng/ml; R&D Systems, Minneapolis, MN) or LPS (0.1 µg/ml) from *Escherichia coli* O111:B4 in HPMEC media for 24 h. Complete experimental groups will include: luminal TNF-α, abluminal TNF-α, luminal LPS, abluminal LPS, and control (fresh HPMEC media). Prior to the 24 h cytokine/endotoxin exposure timepoint, neutrophils will be isolated from whole blood using 1-Step™ Polymorph (Accurate Chemical & Scientific Co., Westbury, NY) as previously described.[51] Neutrophils will be stored at room temperature in Hank's balanced salt solution (HBSS) with added 10 mM 4-(2-hydroxyethyl)-1-piperazineethanesulfonic acid (HEPES) and 5 mg/ml bovine serum albumin (BSA). The HBSS-based buffer is necessary to prevent non-specific leukocyte activation prior to experimentation while maintaining cell viability. Neutrophils will be used within 5 hours post-blood draw. For migration experiments, neutrophils will be transferred to 37°C HPMEC media at a concentration of 4.5 million cells/mL and perfused into the luminal chamber of the cytokine/endotoxin exposed µSiM-PVB. The µSiM-PVBs will then be loaded in a stage-top incubator (37°C, 5% CO_2) and phase contrast time-lapse images will be recorded (8 fpm for 30 min). Resulting frames will be imported into the custom designed MATLAB code described in **Task 2.1**. Data collection will be focused on extracting the following parameters: Luminal neutrophil velocity (mean and median), abluminal neutrophil velocity (mean and median), normalized neutrophil transmigration, and luminal neutrophil chemotactic index (CI), where CI is defined as the ratio of mean cell displacement, <d>, to total path length, L_{path} (Equation 4).[52]

$$CI = \frac{\langle d \rangle}{L_{Path}} \tag{4}$$

We will also record the ratio of neutrophil transmigration spots to total transmigration events to provide insight on 'hotspots' (instances of multiple transmigration events through a single location), and time progression of transmigration events.

Task 2.3: **Identify mediators of a polarized response to cytokine and endotoxin *in vitro*.** TNF-α and LPS exposed µSiM-PVBs will be prepared as described in **Task 2.2**. Following 24 h cytokine/endotoxin incubation, µSiM-PVBs will be utilized to study neutrophil extravasation factors and their influence on polarized cytokine/endotoxin driven neutrophil dynamics. First, we will explore the influence of TNF-α and LPS on intracellular adhesion molecule 1 (ICAM-1) expression using an *in situ* immunocytochemistry (ICC) approach. Briefly, live treated ECs will be blocked with 10% BSA in imaging buffer for 1 h, and subsequently incubated with PE-conjugated anti-ICAM-1 with human reactivity for 30 min. Devices will be transferred to an inverted epifluorescence microscope and images will be recorded in technical triplicate in random locations atop the porous membrane. Grayscale values will be quantified in FIJI and averaged across technical replicates. Experimental triplicates will be performed. Grayscale values approximating ICAM-1 expression will be statistically compared across groups using a pairwise t-test. Similar approaches will be utilized to explore influences of polarized cytokine/endotoxin on PECAM-1 and VE-Cadherin expression and localization. Permeability assays as described in **Task 1.3** will be utilized to probe for effects on EC monolayer integrity. The use of blocking/neutralizing antibodies will aid in mechanistic discovery. For example, if PECAM-1 ICC shows semi-quantitative variability between

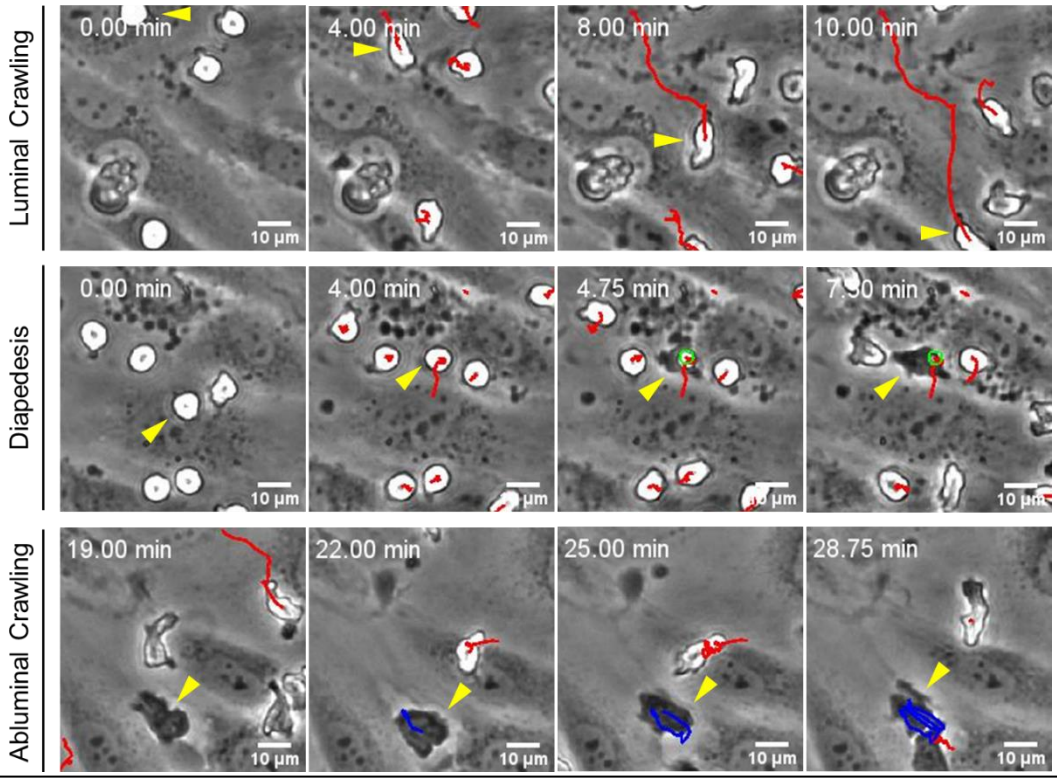

Figure 6. Modified particle tracking algorithm permits unbiased tracking of luminal and abluminal neutrophil dynamics, as well as instances of neutrophil transmigration. Spatial and temporal data is recorded and subsequently analyzed for characteristics of the innate immune response (rolling, crawling, and diapedesis). This data will be predictive of what aspects of the neutrophil extravasation cascade are being regulated.

experimental groups, PECAM-1 blocking Abs and respective isotype controls will be incubated with neutrophils prior to their introduction to the treated EC layers, and tracking experiments will be repeated. This approach will allow us to determine the importance of the respective mediator in a highly controlled environment. The final study within this task will probe the ECs ability to secrete IL-8, a potent chemotactic factor,[53,54] in a polarized manor. Cell culture supernatant will be pulled from apical and basal channels and probed for IL-8 content using a sensitive enzyme-linked immunosorbent assay (ELISA) with IL-8 specificity. These studies will ultimately aim to elucidate a targetable mechanism of polarized cytokine/endotoxin driven immune responses.

Expected Outcomes

With the completion of this aim, we expect to demonstrate the utility of our µSiM-PVB platform in observing real time leukocyte dynamics under polarized cytokine and endotoxin delivery. We expect the results to elucidate differences between barrier and neutrophil trafficking responses to “tissue” vs “blood” mediators of inflammation. In so doing, we may inform pharmaceutical development by providing an immune response target that is sensitive to systemic inflammation, without completely halting the host immune response to local, pathogenic infections. With TNF-α and LPS playing significant roles in the onset and progression of sepsis,[6,11,55] we believe these data will directly inform sepsis therapeutic strategies going forward. These results may also suggest the benefits of studying EC apicobasal polarity for enhanced drug development as proposed in the coming aim.

Potential Problems and Alternative Strategies

While preliminary data has shown early success in the implementation of the particle tracking algorithm for leukocyte dynamics, we anticipate difficulties in accurately distinguishing the transmigration events and their locations. Specifically, the current algorithm utilizes an iterative tracking technique to locate

instances of cells changing from phase white (luminal crawling) to phase dark (abluminal crawling). In some cases, this transition can take place over a few frames, or lag over 10-20. This variability increases the chance of missing a transmigration event, while also increasing the chance of the algorithm to mistake a phase dark cell passing by a phase white cell as a transmigration event. To overcome this issue, we propose the use of image analysis tools to hand track the transmigration events. At the current leukocyte perfusion density, we anticipate roughly 15-25 transmigration events in a single time lapse. In the freeware FIJI, time lapse videos can be overlaid with a grid pattern and transmigration events can be marked using the cell counter plugin. This technique will provide spatial and temporal data on all transmigration events, which can then be analyzed in MATLAB. These data will be combined with luminal and abluminal crawling tracks to form the complete data set as proposed.

In order to assess endothelial permeability, we propose the use of a novel *in situ* permeability technique in which FITC-dextran flux is monitored overtime as developed in **Task 1.3**. In any case if the resistance due to the system is greater than the resistance due to the EC monolayer, the permeability measurements may be indistinguishable from system noise. We plan to overcome this by utilizing a small path length to the detector. However, in the case that difficulties arise in this configuration, we propose the use of the well-established TEER method for evaluating permeability in a Transwell™ culture system. While these data will not directly mimic the permeability within our µSiM-PVB system, we believe it will directly inform our study, and support our conclusions.

Aim 3: Demonstrate the polarized dependence of S1P in regulating pulmonary vasculature permeability following septic insult *in vitro*.

Hypothesis and Rationale: S1P is a bioactive phosphosphingolipid with known physiological and pathophysiological roles in many aspects of vasculature biology including angiogenesis, barrier integrity, and inflammation.[17,18,56-58] A recent study emphasized S1P as a potential biomarker in sepsis: decreased serum S1P levels proved to be a stronger predicter of septic shock than SOFA score[59] as determined by a multivariate logistic regression model.[14] To date, much research has focused on the role of S1P in acute lung injury (ALI) and acute respiratory distress syndrome (ARDS),[15,16,56,60] both when sepsis-associated and trauma induced. S1P interacts with immune cells and ECs alike through their 5 G-protein coupled receptors (SIPR1-5).[61] Interestingly, there appears to be a paradox in S1P physiology, as interactions with its first receptor, S1PR1, increases vasculature barrier properties, signaling through the RAC pathway to promote adherence junctions,[14,56,60,61] while binding of its third GPCR, S1PR3, has shown to increase leukocyte egress and thus vasculature permeability, signaling through the RHO-ROCK pathway to disrupt adherence junctions.[15,16,62] Recently, immunostaining revealed a possible polarized expression of S1P receptors; while S1PR1 was expressed on both the luminal and abluminal surface of rat brain capillaries, S1PR3 expression appears localized to the luminal surface.[63] Together, this data supports a hypothesis that targeted delivery of S1P to the abluminal surface of the microvasculature may isolate the barrier enhancing properties of S1P therapeutics.

Task 3.1: Develop a protocol for incorporating human serum into our vasculature mimetic. In this task, we will characterize and optimize the use of human serum in our vasculature mimetic. Cell culture experiments to date have been performed in fetal bovine serum (FBS) supplemented media. In order to examine the effects of human serum on our ECs, FBS (-) HPMEC media will be spiked with healthy human serum at varying concentrations (5, 10, 15, and 20%). Cell viability and proliferation will be scored 48 hours following human serum media perfusion using a live/dead viability/cytotoxicity immunocytochemistry kit (BioVision Inc., Milpitas, CA). Viability and proliferation counts will be compared to cells treated with FBS spiked MCDB-131 (control). We anticipate minimal effects of healthy human serum on cell proliferation and viability within our concentration range. Human serum concentration resulting in the least deviation from proliferation and viability seen with tradition FBS media will be selected for subsequent experimentation to maintain consistency (paired t-test for significance).

Task 3.2: Investigate the polarized effects of S1P in regulating neutrophil trafficking and pulmonary vasculature leakage following clinical septic serum challenge. Serum samples from ICU administered patients at the University of Rochester Strong Memorial Hospital with confirmed diagnosis of sepsis will be collected as follows: whole blood will be drawn by venipuncture into heparin-containing vacutainer tubes and centrifuged at 1500g for 10 min. Plasma supernatant will be isolated and immediately frozen at - 80 °C until experiments may be performed. Samples from healthy volunteers will be isolated and banked in an identical fashion. SOFA score as determined at point of blood draw will be used to place patients into categories based on sepsis severity. SOFA scores ranging from 1-7, 7-11, and > 11 will be considered low, medium, and high severity sepsis for experimentation purposes. For reference, healthy subjects will have a SOFA score of 0 upon blood draw. Prior to serum thawing, the μSiM-PVB will be prepared, and shear conditioned as preciously described. Following shear priming, serum samples will be warmed to 37 °C and combined with FBS (-) HPMEC media at a concentration determined in **Task 3.1**. Partial serum aliquots will be taken and stored for cytokine analysis (Human Cytokine Array Kit; R&D Systems). The serum challenged μSiM-PVBs will be probed for relative permeability (**Task 1.3)** and neutrophil trafficking (**Tasks 2.1** and **2.2)** simultaneously using an automated microscope stage and shutter. In a parallel replicate, enzymatically produced S1P (Sigma) will be introduced at clinically relevant concentrations (500-1000 nmol/l[14]) either luminally or abluminally following septic insult. Barrier recovery and neutrophil trafficking will be reassessed after 30 min.

Expected Outcomes

This aim will ultimately demonstrate the utility of our μSiM-PVBs platform to elucidate novel therapeutic strategies to combat the maladaptive immune response and debilitating vascular damage seen in sepsis. By exploiting the polarized expression patterns of S1P receptors seen *in vivo*, we expect to counteract the deteriorating effects of septic serum on vascular barrier function in our lung mimetics. Furthermore, we anticipate that this approach will suggest new approaches to systemic treatment in sepsis, possibly by packaging S1P in 'trojan horse' delivery systems that pass-through barriers and release S1P from the 'tissue' side of the PVB.

Potential Problems and Alternative Strategies

Sepsis is a transient disease with many different onsets and paths to mortality or disease resolution. By utilizing clinical septic serum samples over exogenous cytokine delivery, we increase the physiological and clinical relevance of our conclusions. To this means, isolation of clinical serum samples is stochastic, therefore the immediate use of those samples is not practical. We propose the use of banked samples stored at - 80 °C to overcome this issue. There is potential that variability in sample preparation and storage can bias our results; by utilizing a single collection site with strict isolation protocols, we hope to minimize sample variation due to handling.

Proposed Timeline

Aim 1, Task 1 has been completed and published in SMALL.[38] High-throughput fabrication of the static μSiM platform was developed in collaboration with Professor Edward Schwarz's lab and Aline Inc. and is under review for publication. A manufactured flow module is being developed in collaboration with SiMPore and Professor Vinay Abhyankar of RIT and should be complete by the end of 2019. We expect to complete our work developing *in situ* small molecule permeability assays in April and include it in a manuscript that has been already drafted for submission. Work with TNF-α as proposed in Aim 2 is nearing completion, while LPS work is yet to come. We anticipate 8-12 months' work remaining on Aim 2. We expect an additional 12-15 months for the completion of Aim 3. This would complete the thesis by Spring of 2021.

References

1 Singer, M., Deutschman, C. S., Seymour, C. & et al. The third international consensus definitions for sepsis and septic shock (sepsis-3). *JAMA* **315**, 801-810, doi:10.1001/jama.2016.0287 (2016).

2 Aird, W. C. The role of the endothelium in severe sepsis and multiple organ dysfunction syndrome. *Blood* **101**, 3765-3777, doi:10.1182/blood-2002-06-1887 (2003).

3 Hotchkiss, R. S. *et al.* Sepsis and septic shock. *Nat Rev Dis Primers* **2**, 16045, doi:10.1038/nrdp.2016.45 (2016).

4 Reddy, R. C. & Standiford, T. J. Effects of sepsis on neutrophil chemotaxis. *Curr Opin Hematol* **17**, 18-24, doi:10.1097/MOH.0b013e32833338f3 (2010).

5 Colbert, J. F. & Schmidt, E. P. Endothelial and Microcirculatory Function and Dysfunction in Sepsis. *Clin Chest Med* **37**, 263-275, doi:10.1016/j.ccm.2016.01.009 (2016).

6 Lolis, E. & Bucala, R. Therapeutic approaches to innate immunity: severe sepsis and septic shock. *Nat Rev Drug Discov* **2**, 635-645, doi:10.1038/nrd1153 (2003).

7 Gotts, J. E. & Matthay, M. A. Sepsis: pathophysiology and clinical management. *BMJ* **353**, i1585, doi:10.1136/bmj.i1585 (2016).

8 Gaieski, D. F., Edwards, J. M., Kallan, M. J. & Carr, B. G. Benchmarking the incidence and mortality of severe sepsis in the United States. *Crit Care Med* **41**, 1167-1174, doi:10.1097/CCM.0b013e31827c09f8 (2013).

9 van der Poll, T., van de Veerdonk, F. L., Scicluna, B. P. & Netea, M. G. The immunopathology of sepsis and potential therapeutic targets. *Nature Reviews Immunology* **17**, 407, doi:10.1038/nri.2017.36 (2017).

10 Ware, L. B. & Matthay, M. A. The acute respiratory distress syndrome. *N Engl J Med* **342**, 1334-1349, doi:10.1056/NEJM200005043421806 (2000).

11 Russell, J. A., Rush, B. & Boyd, J. Pathophysiology of Septic Shock. *Crit Care Clin* **34**, 43-61, doi:10.1016/j.ccc.2017.08.005 (2018).

12 Kim, W. Y. & Hong, S. B. Sepsis and Acute Respiratory Distress Syndrome: Recent Update. *Tuberc Respir Dis (Seoul)* **79**, 53-57, doi:10.4046/trd.2016.79.2.53 (2016).

13 Sheu, C. C. *et al.* Clinical characteristics and outcomes of sepsis-related vs non-sepsis-related ARDS. *Chest* **138**, 559-567, doi:10.1378/chest.09-2933 (2010).

14 Winkler, M. S. *et al.* Decreased serum concentrations of sphingosine-1-phosphate in sepsis. *Crit Care* **19**, 372, doi:10.1186/s13054-015-1089-0 (2015).

15 Sun, X. *et al.* Sphingosine-1-phosphate receptor-3 is a novel biomarker in acute lung injury. *Am J Respir Cell Mol Biol* **47**, 628-636, doi:10.1165/rcmb.2012-0048OC (2012).

16 Sun, X. *et al.* Functional promoter variants in sphingosine 1-phosphate receptor 3 associate with susceptibility to sepsis-associated acute respiratory distress syndrome. *American journal of physiology. Lung cellular and molecular physiology* **305**, L467-477, doi:10.1152/ajplung.00010.2013 (2013).

17 Tsai, H. C. & Han, M. H. Sphingosine-1-Phosphate (S1P) and S1P Signaling Pathway: Therapeutic Targets in Autoimmunity and Inflammation. *Drugs* **76**, 1067-1079, doi:10.1007/s40265-016-0603-2 (2016).

18 Spiegel, S. & Milstien, S. The outs and the ins of sphingosine-1-phosphate in immunity. *Nat Rev Immunol* **11**, 403-415, doi:10.1038/nri2974 (2011).

19 DesOrmeaux, J. P. *et al.* Nanoporous silicon nitride membranes fabricated from porous nanocrystalline silicon templates. *Nanoscale* **6**, 10798-10805, doi:10.1039/c4nr03070b (2014).

20 Mossu, A. *et al.* A silicon nanomembrane platform for the visualization of immune cell trafficking acros the human blood-brain barier under flow. *Journal of Cerebral Blood Flow & Metabolism* (2018).

21 Carter, R. N. *et al.* Ultrathin transparent membranes for cellular barrier and co-culture models. *Biofabrication* **9**, 015019, doi:10.1088/1758-5090/aa5ba7 (2017).

22 Burgin, T., Johnson, D., Chung, H., Clark, A. & McGrath, J. Analytical and Finite Element Modeling of Nanomembranes for Miniaturized, Continuous Hemodialysis. *Membranes* **6**, doi:10.3390/membranes6010006 (2015).

23 Santaguida, S. *et al.* Side by side comparison between dynamic versus static models of blood-brain barrier in vitro: a permeability study. *Brain Res* **1109**, 1-13, doi:10.1016/j.brainres.2006.06.027 (2006).
24 Booth, R. & Kim, H. Characterization of a microfluidic in vitro model of the blood-brain barrier (muBBB). *Lab Chip* **12**, 1784-1792, doi:10.1039/c2lc40094d (2012).
25 Muller, W. A. & Luscinskas, F. W. Assays of Transendothelial Migration in vitro. *Methods in enzymology* **443**, 155-176, doi:10.1016/S0076-6879(08)02009-0 (2008).
26 Striemer, C. C., Gaborski, T. R., McGrath, J. L. & Fauchet, P. M. Charge- and size-based separation of macromolecules using ultrathin silicon membranes. *Nature* **445**, 749-753, doi:10.1038/nature05532 (2007).
27 Worzfeld, T. & Schwaninger, M. Apicobasal polarity of brain endothelial cells. *J Cereb Blood Flow Metab* **36**, 340-362, doi:10.1177/0271678X15608644 (2016).
28 Zovein, A. C. *et al.* Beta1 integrin establishes endothelial cell polarity and arteriolar lumen formation via a Par3-dependent mechanism. *Developmental cell* **18**, 39-51, doi:10.1016/j.devcel.2009.12.006 (2010).
29 Muller, W. A. & Gimbrone, M. A., Jr. Plasmalemmal proteins of cultured vascular endothelial cells exhibit apical-basal polarity: analysis by surface-selective iodination. *J Cell Biol* **103**, 2389-2402 (1986).
30 van Buul-Wortelboer, M. F., Brinkman, H. J., Reinders, J. H., van Aken, W. G. & van Mourik, J. A. Polar secretion of von Willebrand factor by endothelial cells. *Biochim Biophys Acta* **1011**, 129-133 (1989).
31 Lizama, C. O. & Zovein, A. C. Polarizing pathways: balancing endothelial polarity, permeability, and lumen formation. *Exp Cell Res* **319**, 1247-1254, doi:10.1016/j.yexcr.2013.03.028 (2013).
32 McCloskey, R. V., Straube, R. C., Sanders, C., Smith, S. M. & Smith, C. R. Treatment of septic shock with human monoclonal antibody HA-1A. A randomized, double-blind, placebo-controlled trial. CHESS Trial Study Group. *Annals of internal medicine* **121**, 1-5 (1994).
33 Ziegler, E. J. *et al.* Treatment of gram-negative bacteremia and shock with human antiserum to a mutant Escherichia coli. *N Engl J Med* **307**, 1225-1230, doi:10.1056/nejm198211113072001 (1982).
34 Fisher, C. J., Jr. *et al.* Treatment of septic shock with the tumor necrosis factor receptor:Fc fusion protein. The Soluble TNF Receptor Sepsis Study Group. *N Engl J Med* **334**, 1697-1702, doi:10.1056/nejm199606273342603 (1996).
35 Gray, K. M. & Stroka, K. M. Vascular endothelial cell mechanosensing: New insights gained from biomimetic microfluidic models. *Semin Cell Dev Biol* **71**, 106-117, doi:10.1016/j.semcdb.2017.06.002 (2017).
36 Mazzocchi, A. R., Man, A. J., DesOrmeaux, J.-P. S. & Gaborski, T. R. Porous Membranes Promote Endothelial Differentiation of Adipose-Derived Stem Cells and Perivascular Interactions. *Cellular and Molecular Bioengineering* **7**, 369-378, doi:10.1007/s12195-014-0354-7 (2014).
37 Casillo, S. M., Peredo, A. P., Perry, S. J., Chung, H. H. & Gaborski, T. R. Membrane Pore Spacing Can Modulate Endothelial Cell-Substrate and Cell-Cell Interactions. *ACS Biomater Sci Eng* **3**, 243-248, doi:10.1021/acsbiomaterials.7b00055 (2017).
38 Salminen, A. T. *et al.* Ultrathin Dual-Scale Nano- and Microporous Membranes for Vascular Transmigration Models. *Small* **0**, 1804111, doi:doi:10.1002/smll.201804111.
39 Agrawal, A. A. *et al.* Porous nanocrystalline silicon membranes as highly permeable and molecularly thin substrates for cell culture. *Biomaterials* **31**, 5408-5417, doi:10.1016/j.biomaterials.2010.03.041 (2010).
40 Nehilla, B. J., Nataraj, N., Gaborski, T. R. & McGrath, J. L. Endothelial vacuolization induced by highly permeable silicon membranes. *Acta biomaterialia* **10**, 4670-4677, doi:10.1016/j.actbio.2014.07.022 (2014).
41 Ishimatsu, R. *et al.* Ion-selective permeability of an ultrathin nanoporous silicon membrane as probed by scanning electrochemical microscopy using micropipet-supported ITIES tips. *Anal Chem* **82**, 7127-7134, doi:10.1021/ac1005052 (2010).

42 Khire, T. S. Silicon Nanomembranes for Advanced Microvascular Mimetics. *PhD Thesis Document* (2018).
43 Monaghan-Benson, E. & Wittchen, E. S. In vitro analyses of endothelial cell permeability. *Methods in molecular biology (Clifton, N.J.)* **763**, 281-290, doi:10.1007/978-1-61779-191-8_19 (2011).
44 Crank, J. *The mathematics of diffusion / by J. Crank*. (Clarendon Press, 1975).
45 Ziegler, E. J. *et al.* Treatment of Gram-Negative Bacteremia and Septic Shock with HA-1A Human Monoclonal Antibody against Endotoxin. *New England Journal of Medicine* **324**, 429-436, doi:10.1056/nejm199102143240701 (1991).
46 Dickinson, C. M. *et al.* Leukadherin-1 ameliorates endothelial barrier damage mediated by neutrophils from critically ill patients. *Journal of intensive care* **6**, 19, doi:10.1186/s40560-018-0289-5 (2018).
47 Kim, D. & Haynes, C. L. Neutrophil chemotaxis within a competing gradient of chemoattractants. *Anal Chem* **84**, 6070-6078, doi:10.1021/ac3009548 (2012).
48 Mestre, H. *et al.* Flow of cerebrospinal fluid is driven by arterial pulsations and is reduced in hypertension. *Nat Commun* **9**, 4878, doi:10.1038/s41467-018-07318-3 (2018).
49 H. Kelley, D. & T. Ouellette, N. *Using Particle Tracking to Measure Flow Instabilities in an Undergraduate Laboratory Experiment*. Vol. 79 (2011).
50 T. Ouellette, N., Xu, H. & Bodenschatz, E. *A quantitaive study of three-dimensional Lagrangian particle tracking algorithms*. Vol. 40 (2006).
51 Chung, H. H. *et al.* Highly permeable silicon membranes for shear free chemotaxis and rapid cell labeling. *Lab Chip* **14**, 2456-2468, doi:10.1039/c4lc00326h (2014).
52 Lauffenburger, D. A. L., J. L. *Receptors*. (Oxford University Press, Inc., 1993).
53 Mukaida, N. Pathophysiological roles of interleukin-8/CXCL8 in pulmonary diseases. *American journal of physiology. Lung cellular and molecular physiology* **284**, L566-577, doi:10.1152/ajplung.00233.2002 (2003).
54 Smart, S. J. & Casale, T. B. TNF-alpha-induced transendothelial neutrophil migration is IL-8 dependent. *Am J Physiol* **266**, L238-245, doi:10.1152/ajplung.1994.266.3.L238 (1994).
55 Murphy, K. & Weaver, C. *Janeway's immunobiology*. Ninth edn, 77-137 (Garland Science).
56 Natarajan, V. *et al.* Sphingosine-1-phosphate, FTY720, and sphingosine-1-phosphate receptors in the pathobiology of acute lung injury. *Am J Respir Cell Mol Biol* **49**, 6-17, doi:10.1165/rcmb.2012-0411TR (2013).
57 Camerer, E. *et al.* Sphingosine-1-phosphate in the plasma compartment regulates basal and inflammation-induced vascular leak in mice. *J Clin Invest* **119**, 1871-1879 (2009).
58 Kono, M., Allende, M. L. & Proia, R. L. Sphingosine-1-Phosphate Regulation of Mammalian Development. *Biochimica et biophysica acta* **1781**, 435-441, doi:10.1016/j.bbalip.2008.07.001 (2008).
59 Vincent, J. L. Organ dysfunction in patients with severe sepsis. *Surgical infections* **7 Suppl 2**, S69-72, doi:10.1089/sur.2006.7.s2-69 (2006).
60 Sun, X. *et al.* Functional variants of the sphingosine-1-phosphate receptor 1 gene associate with asthma susceptibility. *J Allergy Clin Immunol* **126**, 241-249, 249 e241-243, doi:10.1016/j.jaci.2010.04.036 (2010).
61 Winkler, M. S. *et al.* Sphingosine-1-Phosphate: A Potential Biomarker and Therapeutic Target for Endothelial Dysfunction and Sepsis? *Shock (Augusta, Ga.)* **47**, 666-672, doi:10.1097/shk.0000000000000814 (2017).
62 Nussbaum, C. *et al.* Sphingosine-1-phosphate receptor 3 promotes leukocyte rolling by mobilizing endothelial P-selectin. *Nat Commun* **6**, 6416, doi:10.1038/ncomms7416 (2015).
63 Cannon, R. E., Peart, J. C., Hawkins, B. T., Campos, C. R. & Miller, D. S. Targeting blood-brain barrier sphingolipid signaling reduces basal P-glycoprotein activity and improves drug delivery to the brain. *Proc Natl Acad Sci U S A* **109**, 15930-15935, doi:10.1073/pnas.1203534109 (2012).

Appendix

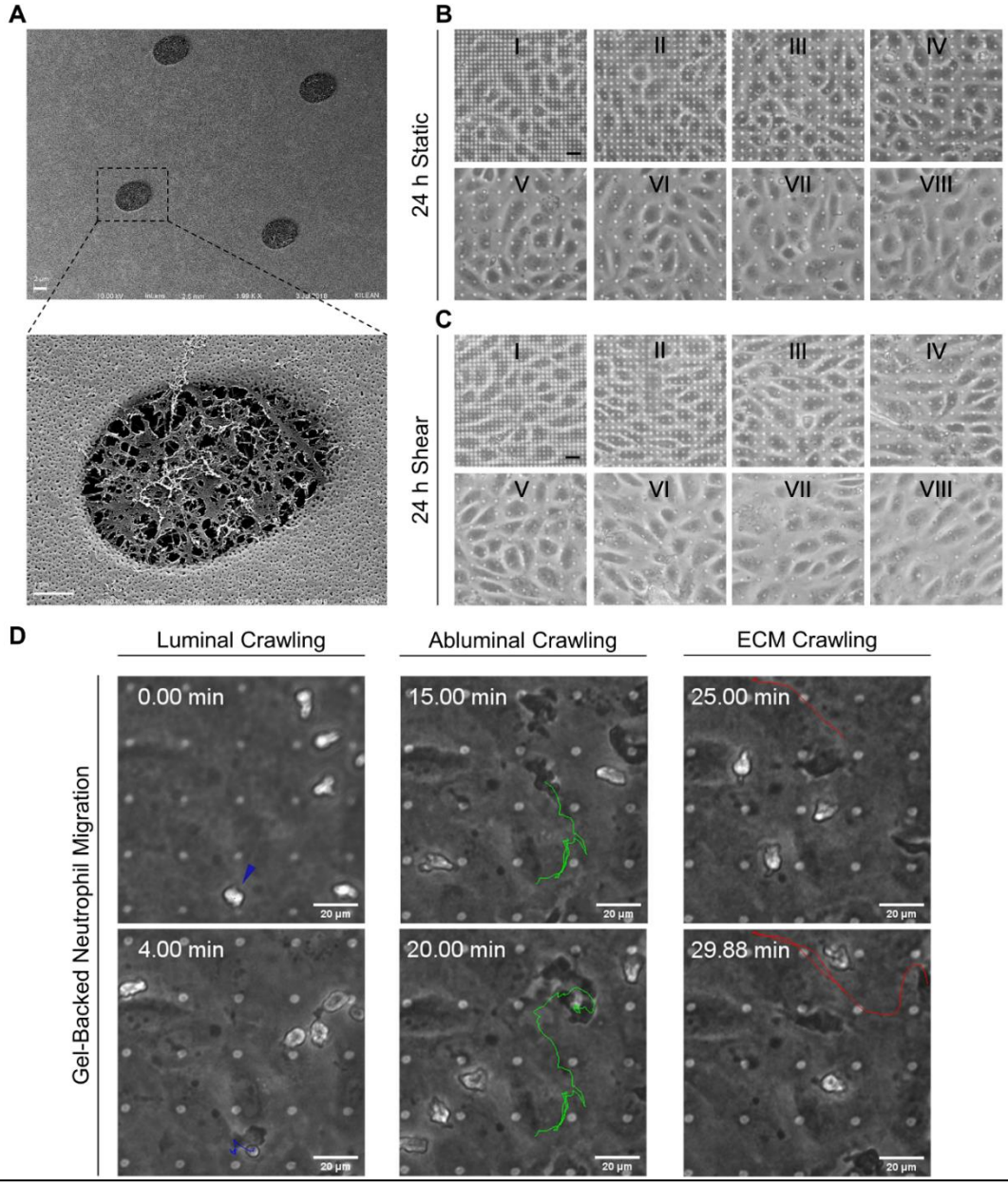

Supplemental Figure 1. Sub-membrane collagen maintains endothelial monolayer for a variety of micropore densities. A 300 µm collagen gel was added to the basal side of a dual-scale (nano- and micro-porous) membrane. (A) SEM images were obtained of glutaraldehyde fixed samples without cells (Top Scale bar = 2 µm; Bottom Scale bar = 1 µm). (B) Phase images were obtained of human umbilical vein endothelial cells (HUVECs) seeded on collagen gel back dual-scale membranes grown over 24 h (Scale bar = 20 µm). (C) Additionally, HUVECs seeded on gel back dual-scale membranes were grown to confluency and sheared at 4.5 dyn/cm^2 for 24 h and phase images were recorded (Scale bar = 20 µm). Roman numerals in panels B and C correspond to the following 3 µm pore densities (pores/mm^2): I = 27777, II = 12345, III = 6944, IV = 4444, V = 3086, VI = 2267, VII = 1736, VIII = 1371.

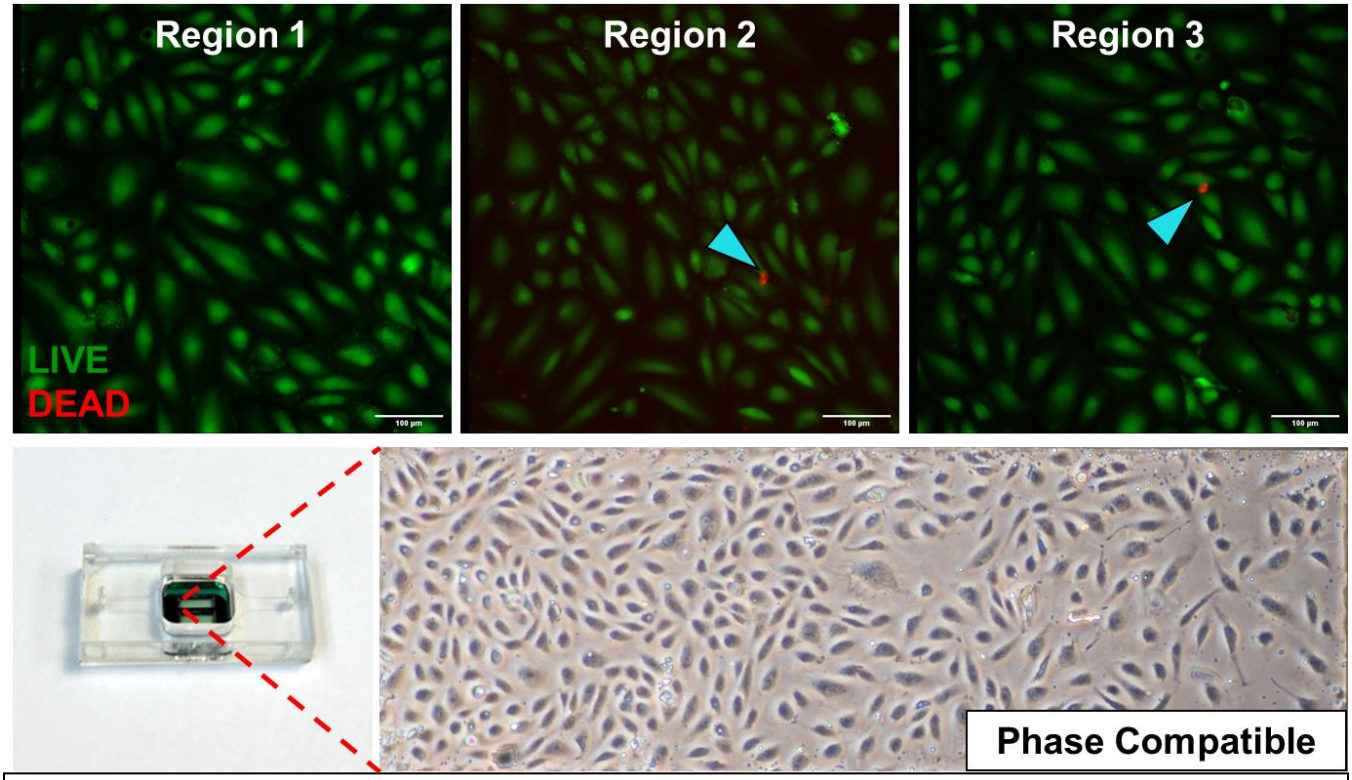

Supplemental Figure 2. High-throughput manufacturing of microfluidic 'transwells' supports human cell viability and clear imaging. HUVECs were seeded in fibronectin (5 µg/ml) coated Aline-produced devices. Cells were maintained in culture at 37°C/5% CO_2 for 48 h with media changes every 24 h. Cells were examined for viability using a Live/Dead Cell Viability Assay Kit (BioVision Inc.) In three representative fields of view, live cells were abundant (green) while minimal dead cells were found (red), demonstrating the biocompatibility of the devices over 48 h cultures. The low working distance to the membrane supporting the cells permits clear phase contrast imaging for continuous cell monitoring without the need for exogenous dyes.

NANO · MICRO small
www.small-journal.com

Ultrathin Dual-Scale Nano- and Microporous Membranes for Vascular Transmigration Models

Alec T. Salminen, Jingkai Zhang, Gregory R. Madejski, Tejas S. Khire, Richard E. Waugh, James L. McGrath, and Thomas R. Gaborski**

Selective cellular transmigration across the microvascular endothelium regulates innate and adaptive immune responses, stem cell localization, and cancer cell metastasis. Integration of traditional microporous membranes into microfluidic vascular models permits the rapid assay of transmigration events but suffers from poor reproduction of the cell permeable basement membrane. Current microporous membranes in these systems have large nonporous regions between micropores that inhibit cell communication and nutrient exchange on the basolateral surface reducing their physiological relevance. Here, the use of 100 nm thick continuously nanoporous silicon nitride membranes as a base substrate for lithographic fabrication of 3 μm pores is presented, resulting in a highly porous (≈30%), dual-scale nano- and microporous membrane for use in an improved vascular transmigration model. Ultrathin membranes are patterned using a precision laser writer for cost-effective, rapid micropore design iterations. The optically transparent dual-scale membranes enable complete observation of leukocyte egress across a variety of pore densities. A maximal density of ≈14 micropores per cell is discovered beyond which cell–substrate interactions are compromised giving rise to endothelial cell losses under flow. Addition of a subluminal extracellular matrix rescues cell adhesion, allowing for the creation of shear-primed endothelial barrier models on nearly 30% continuously porous substrates.

1. Introduction

Leukocytes, metastatic cancer cells, and recruited stem cells use the vasculature system to access peripheral tissues in vivo.[1–4] Transport into and out of the blood vessels (extravasation) is regulated by endothelial cells (ECs), pericytes, perivascular extracellular matrix (ECM), resident innate immune cells, and a variety of cytokine signals, all working to maintain or restore vascular barrier homeostasis. The study of leukocyte egress through the vascular wall is the most widely studied transmigration event.[5] Pathogen-associated molecular patterns (PAMPs) trigger a response in the innate immune cells primarily residing in the peripheral tissues.[6] These immune cells, such as macrophages, release a variety of cytokine and proinflammatory molecules that stimulate the ECs lining the blood vessels within proximity to the pathogenic invasion. The resulting cytokine gradient, coupled with the expression of pro-transmigration molecules on the EC surface, attracts circulating leukocytes to the site of infection.[7]

As in vivo leukocyte transmigration cannot be viewed directly, current studies implement the use of specialized intravital microscopy systems to observe these events in real time in situ.[8,9] While these methods act as a powerful discovery tool in the field of leukocyte transmigration, unique imaging systems and intensive preimaging surgeries limit the scalability of these studies. The recent development of highly controlled, human cell based in vitro microvasculature models, however, have enabled leukocyte transmigration studies at the lab bench.[10]

Microfluidics-based vascular models have made use of planar microporous membranes as a selective support layer for EC growth.[11–14] These membranes are ideal for transmigration studies as they promote the growth of ECs into a continuous flat monolayer and can have optically favorable properties for real-time imaging. Conveniently, microporous membranes come in many forms (material, pore size, thickness) depending on the intended use.[11] Polyethylene terephthalate membranes with 3 μm pores have been used to facilitate neutrophil transmigration assays through an EC (human umbilical vein ECs (HUVECs)) monolayer.[15] Furthermore, polycarbonate filters with 8 μm and 12 μm pores were utilized to assess the migratory potential of melanoma cell lines.[16] Our lab has also previously developed an ultrathin, optically transparent silicon dioxide (SiO_2) membrane with tunable pore sizes for use in

A. T. Salminen, Dr. G. R. Madejski, T. S. Khire, Dr. R. E. Waugh, Dr. J. L. McGrath, Dr. T. R. Gaborski
Department of Biomedical Engineering
University of Rochester
Rochester, NY 14627, USA
E-mail: jmcgrath@ur.rochester.edu; thomas.gaborski@rit.edu
J. Zhang
Institute of Optics
University of Rochester
Rochester, NY 14627, USA
Dr. T. R. Gaborski
Department of Biomedical Engineering
Rochester Institute of Technology
Rochester, NY 14623, USA
The ORCID identification number(s) for the author(s) of this article can be found under https://doi.org/10.1002/smll.201804111.

DOI: 10.1002/smll.201804111

cell culture systems.[17,18] Further use of planar membranes for organ-on-a-chip platforms has been reviewed in detail elsewhere.[19]

While microporous membranes support monolayer integrity and transmigration events, they may not be ideal substrates when compared to the basement membrane (BM) in vivo. Traditionally, these polymeric and microfabricated membranes contain relatively large non-porous regions between micropores on which cells can adhere and proliferate. In some cases, these non-porous regions can span 40 μm between pores,[20,21] resulting in potentially non-uniform cell signaling and nutrient uptake on the basolateral surface of the endothelial monolayer. In studies aimed at observing subluminal stimulation of ECs or circulating leukocytes, pore non-uniformity could compromise the physiological fidelity of the transmigration model. One solution to this shortcoming is to increase substrate permeability through the addition of tightly-packed pores. In the microporous regime, a significant increase in pore density results in a decrease in membrane structural integrity, increasing the difficulty of integrating these membranes into cell culture devices, especially when physiological membrane thickness is desired.

Increased micropore density can also influence cell function, particularly the ability of the cell monolayer to remain adherent to the substrate under physiological shear forces. Previously, our lab presented the use of microporous silicon membranes as a model vascular substrate.[22] In that study, HUVECs were seeded on microporous membranes with varying pore size and density. It was concluded that an increase in micropore density can result in decreased cell–substrate interactions (as measured by focal adhesion staining).[22] In a recent study of a blood–brain barrier (BBB) model, ECs were found to detach within minutes of the onset of physiological flow on microporous SiO_2 membranes,[23] ultimately guiding the decision to utilize nanoporous membranes for the BBB model. Importantly, others have reported success in maintaining EC monolayers under shear on track-etched (TE) and PDMS microporous membranes.[12,21] This discrepancy, however, may be due to the relatively low pore density and high contact area on TE and PDMS membranes that support stronger cell–substrate interactions. The tradeoff between membrane porosity, thickness, and firm cell adhesion continues to hinder cell barrier research.[24] Considering physiological shear stress is known to modulate EC barrier formation in vitro,[25,26] it is appropriate to conclude it is a necessary condition for the study of transmigration through barrier models. Therefore, to create a robust membrane solution with both high basolateral surface permeability and EC monolayer integrity under shear, it is necessary to change the paradigm of traditional microporous membrane fabrication.

Previously, our lab has developed a variety of ultrathin (50–100 nm), highly permeable nanoporous membranes for use in cell culture,[27–29] and biological separations.[30–32] These membranes contain pores ranging in size from 15 to 100 nm with pore to pore spacing less than 100 nm. While these membranes have been shown to support cell culture despite high porosity, they do not provide pores large enough to permit leukocyte, stem cell, or cancer cell transmigration. However, as demonstrated by Morgan et al., the use of a highly porous material for fabrication of hierarchical support structures allows for drastically increased material porosity without suffering from complete loss of usability.[33] To this end, it may be possible to implement our previously developed nanoporous material as a base substrate for micropore membrane fabrication.

To address the need for improved membrane permeability while simultaneously facilitating transmigration events, we set out to create an ultrathin, dual-scale (nano- and microporous) membrane. We developed methods that enable the lithographic patterning and etching of free-standing ultrathin nanoporous membranes, effectively transferring micropores directly into the highly permeable nanoporous surface. Despite porosities as high as 30%, these membranes provided enough structural integrity to enable integration into microfluidic vascular model systems. We investigated leukocyte transmigration through a variety of pore densities as well as endothelial attachment and retention under shear.

2. Results and Discussion

2.1. Dual-Scale (Nano- and Microporous) Membrane Fabrication and Characterization

To closely mimic the uniform permeability and selective transport of the vascular BM in vitro, we explored the use of the highly porous and ultrathin nanomembrane[34] as the base substrate for microporous membrane fabrication. These membranes are roughly equal in thickness to the BM (≈100 nm),[35] and contain a dense spread of nanopores much like the protein network that constitutes the BM itself.[36] The membrane's uniform permeability can be attributed to the closely packed nanopores (spacing <100 nm)[37] that allow for rapid passage of small molecules and proteins.[31] The addition of micropores to the nanoporous membrane would facilitate motile cell transmigration through a membrane-supported endothelium.

Successful use of novel lithography techniques for vascular model design[38] and membrane fabrication inspired us to explore its use in fabricating dual-scale (nano- and microporous) membranes. Standard lithography processes become more complex when coating an ultrathin, free-standing, porous membrane (**Figure 1**A) in place of a traditional silicon wafer monolith. The proposed lithography process (Figure 1B) begins with the spin coating of the suspended nanomembrane. A consequence of the high rotational velocities necessary to achieve even, thin resist coatings (7000 RPM) is the potential for thin film sag and membrane rupture. Remarkably, the spin coating process did not result in membrane fracture and formed a uniform 500 nm layer of positive photoresist over the entirety of the free-standing and support surfaces. This feat is not without appreciation, as it now opens to the door to an entire bases of lithographic membrane design, all on the surface of a 100 nm thick nanomembrane.

To this end, the photoresist was patterned using a MICRO-TECH LaserWriter system, effectively acting as a pore design template for etching. The use of a laser writer eliminates the need for high resolution mask production, allowing for rapid design iterations. Specifically, the laser writer system is unlimited in nature of design. While the focus of this study was to specifically pattern 3 μm pores for selective leukocyte passage, membranes could potentially be modified with pores of any

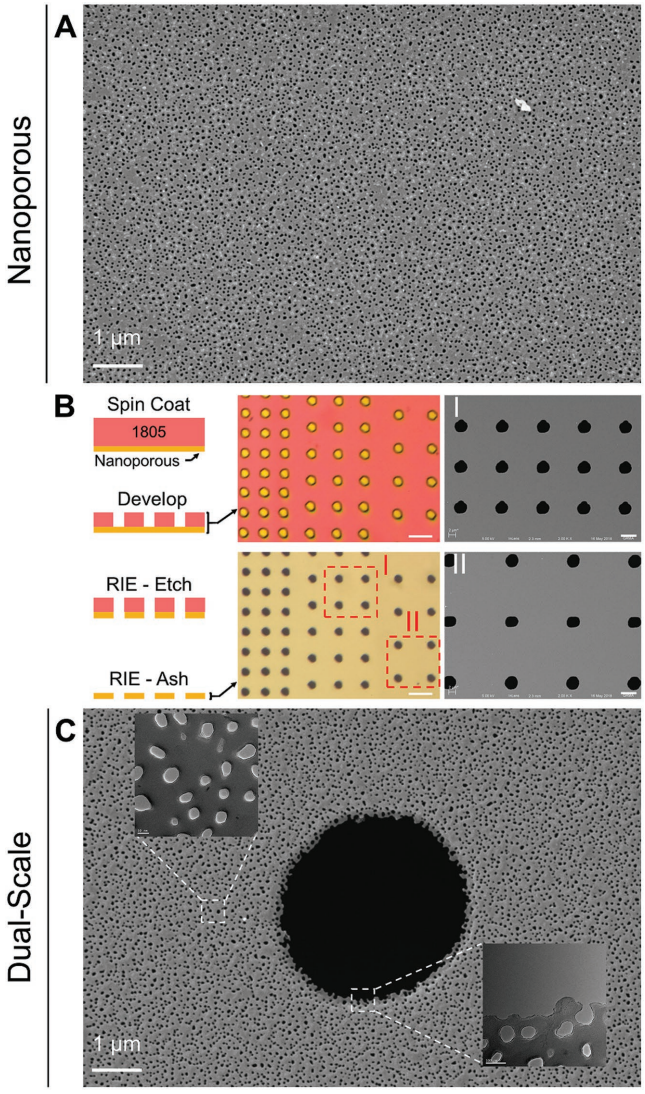

Figure 1. Fabrication of dual-scale porous membranes. A) SEM image of NPN membrane prior to the addition of micropores (scale bar = 1 µm). B) The addition of micropores begins with the spin coating of Shipley 1805 onto the freestanding nanoporous membrane. The 500 nm coating is developed, forming the micropore pattern (scale bar = 10 µm). The pattern is transferred into the nanoporous membrane following an RIE process. The RIE ash process removes the Shipley 1805 mask (scale bar = 10 µm; I, II scale bars = 4 µm). C) SEM image of dual-scale (nano- and microporous) membrane (scale bar = 1 µm). Overlaid TEM images show further membrane detail including nanopore structure and micropore edge.

desired shape (triangle, square, hexagon, etc.) at several varying pore densities. While this may be achievable in other membrane fabrication techniques, our protocol is cost and time effective (≈2 h), and the immediate end result is an ultrathin membrane with the nanoporous background. Furthermore, the laser writer system, allows for in situ alignment, with minimum mechanical stage step sizes in the submicron range. This translates to the ability to precisely pattern micropores at any location on our nanoporous substrate. While it is partially conceptual at this point, a future study may explore the full potential of the patterning techniques described herein. Lastly, a dynamic focus feature of the writer permits consistent exposure over the resist surface, even in the case of resist nonuniformity.

After resist development, the pore pattern was transferred into the free-standing nanoporous membrane using a reactive ion etcher (RIE), and the remaining photoresist was removed with an oxygen plasma ashing step (Figure 1B). The resulting membrane surface contained 3 µm pores etched directly into the highly permeable nanoporous material (dual-scale membranes; Figure 1C, Movie S1, Supporting Information). In using a thin layer of photoresist to protect the nanoporous membrane, there was concern that the resist might have entered the nanopores, making the membrane less permeable following development. We investigated this potential concern with the use of transmission electron microscopy (TEM; Figure 1C). We found that the oxygen plasma was sufficient to remove any residual photoresist. The use of the ash step to remove the photoresist was selected over an acetone wash as it allowed for batch production of the individual membranes, further pushing the rapid prototyping focus of this work.

One potential concern with the reactive ion etch process is the nonspecific etching of the nanoporous substrate, resulting in nanopore enlargement and substrate weakening. Transmission electron micrographs were obtained before (**Figure 2**A) and after (Figure 2B) micropore etching. The pore size distributions in both cases (Figure 2A,B) show a negligible change in pore size distribution (44.6 nm for native, 42.7 nm for postmodification). Furthermore, pore shape and porosity are also relatively unchanged.

Porosities of the dual-scale (nano- and microporous) membranes were determined using Equation (1).

$$\varphi_{\text{total}} = \varphi_{\text{np}}\left(1-\varphi_{\mu\text{p}}\right)+\varphi_{\mu\text{p}} \tag{1}$$

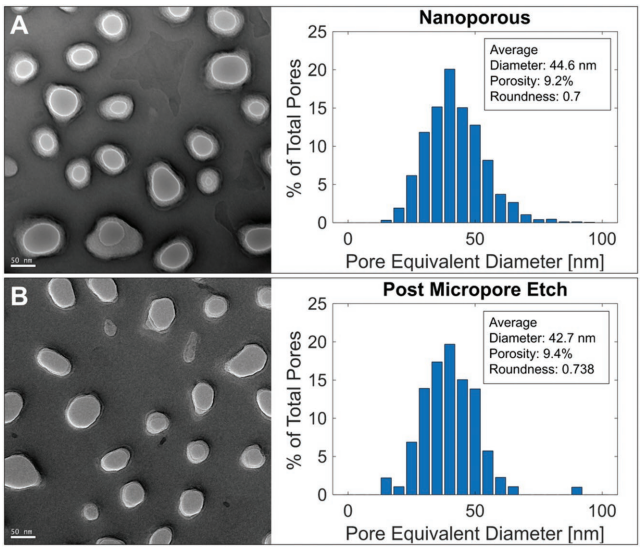

Figure 2. Micropore etching does not alter nanopores. Transmission electron micrographs show pore structure A) before and B) after micropore addition (scale bars = 50 nm). Histograms of pore size were obtained from lower magnification micrographs to obtain a higher pore distribution. Image analysis was performed in MATLAB to obtain average nanopore diameter, porosity, and roundness.

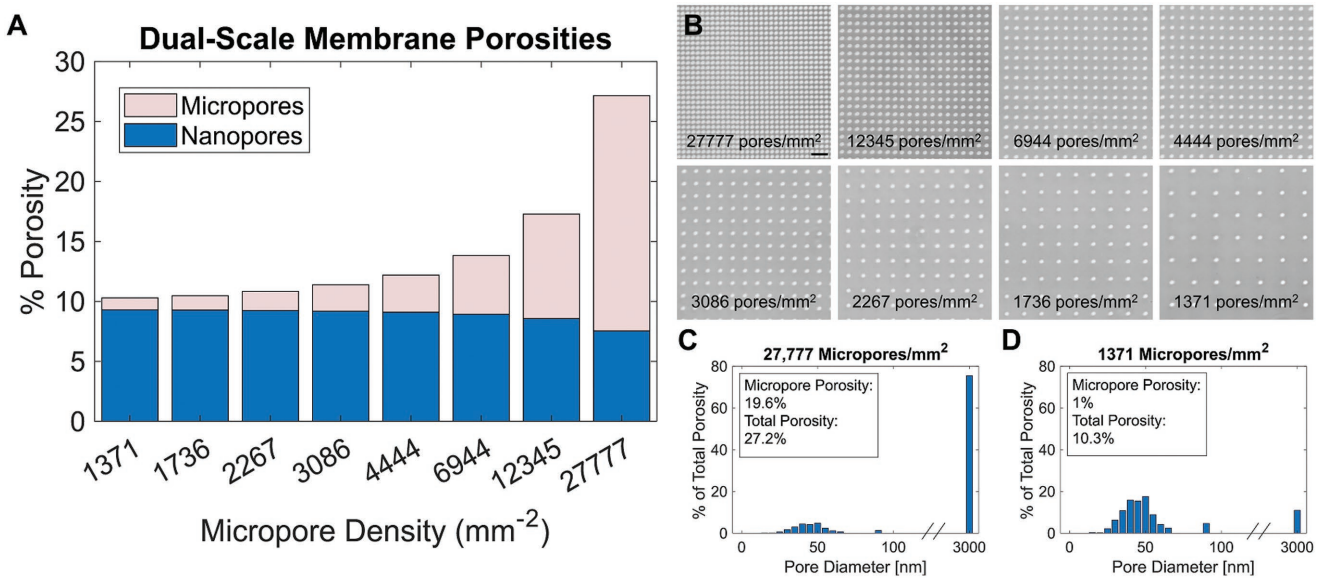

Figure 3. Patterning of micropores. A) Dual-scale membranes were fabricated with eight different micropore patterns and porosities. All micropore patterns are in a square pack configuration. B) Phase images were recorded of all dual-scale membrane varieties (scale bar = 20 µm). Specific pore size contributions to total membrane porosity were determined analytically for C) the highest micropore density and D) lowest micropore density dual-scale membranes.

where φ_{np} represents the porosity of the nanoporous membrane, and $\varphi_{\mu p}$ is the porosity of the equivalent microporous membranes (assuming only micropores). Porosities of all dual-scale membranes can be seen in **Figure 3**A. A unique feature of our dual-scale membranes is the baseline porosity provided by the nanoporous substrate. While porosity invariably declines as micropore density decreases with commercially available TE membrane inserts, the dual-scale membranes presented in Figure 3 are consistently porous (≈10–15%) until the micropore density exceeds 4500 mm^2, at which point the micropores begin to drastically influence membrane porosity. The minimum porosity in this series is 10.3%, very close to the porosity of the underlying nanoporous silicon nitride (NPN; 9.4%) and roughly equivalent to the maximum porosity available for commercial 3 µm pore TE membranes (Corning; 3 µm pores, 2×10^6 pores cm^{-2}). The density of pores in TE membranes are limited by concerns about the merging of the randomly positioned pores,[39] while in our case micropores are precisely positioned on the nanoporous background. When micropore density is highest (27 777 pores mm^{-2}), the total dual-scale membrane porosity is 27.2%, with micropores contributing to three-quarters of this total porosity (Figure 3C). By contrast, micropores contribute only one-tenth of the total membrane porosity at their lowest density (1371 pores mm^{-2}; Figure 3D).

2.2. Leukocyte Transmigration on Nanoporous and Dual-Scale Membranes

The presented porosities of our dual-scale membranes demonstrate the benefits of the combined pore sizes from a material properties perspective. Importantly, the continuity of the nanopores might also have added benefits when making comparisons to the vascular ECM in vivo. The vascular ECM is a network of proteins that supports EC structure and growth. The porous nature of the ECM facilitates cytokine and inflammatory signal delivery directly from the peripheral tissue to the basolateral surface of the EC monolayer.[40] In the case of a strictly microporous membrane, the presence of discrete micropores create artificial "chimneys" that restrict diffusion to highly localized regions of the membrane. In our dual-scale membranes, nanopores permit uniform diffusion of molecules across the endothelial monolayer, much like the in vivo ECM counterpart.

To validate the use of our dual-scale membranes in a leukocyte vascular transmigration model, freshly isolated human neutrophils were introduced to the luminal (top) channel of our cell culture microfluidic device (Figure S1B,C, Supporting Information). Neutrophils settled on the HUVEC monolayer and were attracted to the abluminal (bottom) channel with the addition of *N*-Formylmethionyl-leucyl-phenylalanine (fMLP), a potent chemoattractant. As expected, 3 µm pores facilitated complete neutrophil migration as confirmed by presence of cells on the coverslip 430 µm below the dual-scale porous membrane (abluminal side of device) 30 min post fMLP addition (**Figure 4**B). When unmodified nanoporous membranes were used, the presence of neutrophils was not observed on the coverslip 30 min post fMLP addition (Figure 4A), confirming the necessity of micro-scale pores for complete transmigration. The optical clarity of ultrathin silicon nitride nanomembranes allows for unobstructed phase contrast imaging in situ, unlike TE membranes.[17] With the use of an incubated microscope, neutrophil transmigration experiments were recorded in real time (Figure 4A,B). Progression of neutrophils from phase white to phase dark on both nanoporous and dual-scale (nano- and microporous) membranes highlights the morphological and depth change of neutrophils as they travel underneath the EC monolayer. The observation of neutrophil migration under the monolayer in nanoporous membrane-based

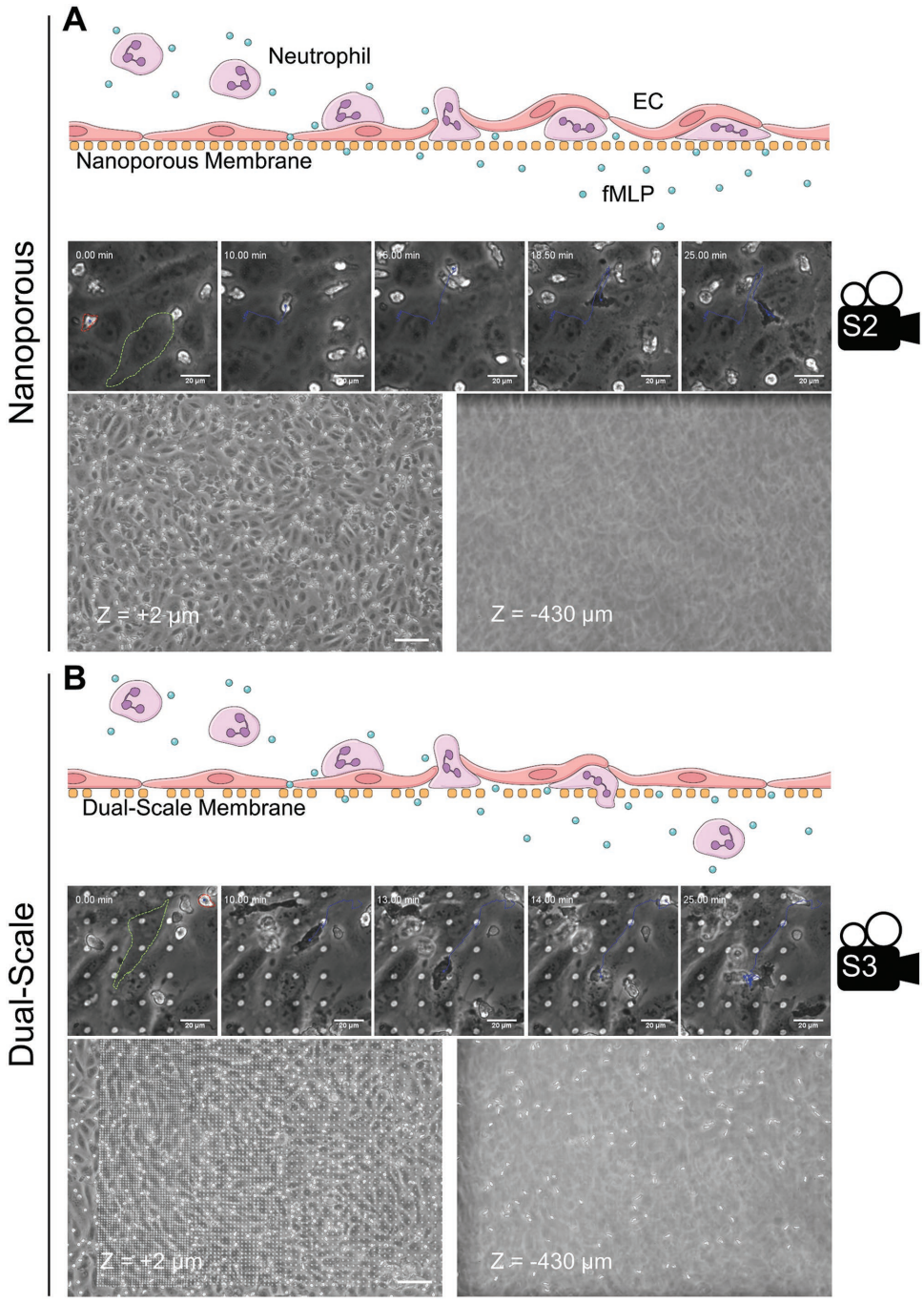

Figure 4. Complete leukocyte transmigration facilitated by dual-scale porous membrane. A) Time-lapse phase contrast images were recorded of neutrophils migrating through a nanoporous membrane supported HUVEC monolayer (scale bars = 20 µm). Representative frames are presented. Phase images were taken 2 µm above the membrane (EC focus) and 430 µm below the membrane (coverslip focus; scale bar = 200 µm) postexperiment to objectively observe neutrophil complete migration. B) Experiments were repeated for dual-scale membranes. Time-lapse videos can be found in the supplemental material.

devices (Figure 4A) eliminates the concern that neutrophils are not exposed to sufficient fMLP to complete transmigration. Furthermore, the real-time imaging of neutrophil migration on dual-scale membranes shows the mechanism of complete transmigration (Figure 4B), in which human neutrophils probe and migrate under the EC monolayer, locate a micropore, and egress through the micropore to reach the abluminal side of the device. The videos of both processes can be seen in Movies S2 and S3 in the Supporting Information. Once under the membrane, neutrophils may crawl, remaining adhered to the silicon nitride membrane, or detach and descend to the abluminal well, as observed by the presence of ripples formed by the motile cells falling out of focus (Movie S4, Supporting Information). Overall, the observable complete migration on dual-scale membranes

demonstrates the power of this platform as a tool for studying vascular transmigration kinetics. The ability for neutrophils to complete migration to the coverslip also adds a level of convenience when conducting experiments that involve quantifying leukocyte (or cancer cell and stem cell) migration. While previous studies explore the use of neutrophil collection and hemocytometer assisted counting of extravasated cells,[41] our mimetic eliminates possible collection error by allowing for in situ counting. Furthermore, the complete transparency of our system from above the EC layer down to the coverslip allows for direct observation of all steps of leukocyte egress. This is especially beneficial when exploring leukocyte regulation, as an observed reduction of neutrophils through the vascular barrier does not inform the study on what step of the transmigration process is halted.[42]

2.3. Cell Adhesion on Varying Micropore Densities Under Shear

Another important aspect of a microphysiological system is the recapitulation of in vivo mechanical stimuli.[24] In the vascular system, this mechanical stimulus can come in many forms, including shear stress, matrix stiffness, and cyclic strain, some of which are more influential depending on the accompanying organ system of interest.[43] Shear stress has presented itself as an important contributor to the formation of a complete EC barrier,[25,26] and has also been hypothesized to influence lymphocyte migration.[44] Shear stress ranges from 4 to 30 dyn cm^{-2} in the arteries, 10 to 20 dyn cm^{-2} in the capillaries, and 1 to 4 dyn cm^{-2} in veins.[45] For our study, we selected a shear stress level of 4.5 dyn cm^{-2}.

Previously, we have observed ECs that had reduced cell–substrate interactions (as measured by focal adhesion staining) as micropore density increased.[22] At the same time, these ECs increased cell–cell interactions (as measured by VE-cadherin staining). This suggests a mechanism by which ECs downregulate their interactions with a highly microporous surface. In the context of a microfluidic shear system, this has indirectly been shown to translate to EC loss under physiological levels of flow.[23] This result is undesired, as it greatly disrupts the establishment of a physiological EC barrier. However, the threshold of micropore densities at which cell–substrate interactions are insufficient to maintain an adherent EC monolayer under shear has yet to be elucidated.

To fill this gap in knowledge, dual-scale membranes with a gradient of micropore densities were designed and fabricated. These membranes contain a ramp of eight different 3 µm pore spacings (6 to 27 µm center to center; **Figure 5**A). The ability to pattern all eight pore spacings on a single free-standing nanoporous membrane permitted highly controlled experiments with all the results in a single field of view. As anticipated, high micropore densities reduced cell–substrate interactions, resulting in EC loss after 24 h exposure to shear (Figure 5A). Postshear cell densities on the highest and lowest micropore densities were equal to 787 and 1172 cells mm^{-2} respectively (Figure 5C). Interestingly, the variation in EC density between micropore densities of 6944 and 1371 pores mm^{-2} was minimal (mean EC density of 1195 cells mm^{-2}, standard deviation of 101 cells mm^{-2}). We hypothesize this is due to the little variation in porosity between these two micropore densities (15.4% vs 10.3%) compared to that of the two extremes (27.2% vs 10.3%).

To address concerns that flow patterns near the entrance or exit of the microfluidic channel might be responsible for patterns of EC loss, side-by-side membranes with different micropore densities were created. Specifically, the highest (27 777 pores mm^{-2}) and lowest (1371 pores mm^{-2}) pore densities tested on the gradient membranes were patterned over the long axis of the nanoporous membrane, resulting in two microporous regions that extended the full length of the membrane (Figure 5B). Once again, EC loss was only observed on the high micropore density region, while cells were retained on the low density micropores Quantification of postshear cell density on gradient dual-scale membranes in Figure 5A revealed a maximal number of micropores per cell of ≈14, above which cell delamination was observed (Figure 5C). This number will provide insight when selecting micropore densities in future shear flow experiments.

2.4. Subluminal Extracellular Matrix Gel for Improved Cell Adhesion

For many transmigration experiments a low density of micropores may be sufficient, especially considering the membranes will still be highly porous because of the nanoporous substrate. For experiments that may need a higher density of micropores and shear priming, these membranes in their bare form may not be suitable. However, the remarkable structural robustness of the dual-scale membrane may permit the use of an underlying physiological matrix to "rescue" the loss of cell adhesion on regions with a high density of micropores. To test this hypothesis, a collagen I gel was added to the abluminal side of the dual-scale membrane, providing additional cell–matrix attachment within the exposed micropores (**Figure 6**A). The collagen gel did not obstruct phase imaging (Figure 6B), and completely rescued cell adhesion on all micropore densities tested following 24 h shear (Figure 6C). The use of an ECM-like gel to back-fill the dual-scale membranes, as opposed to a continuously nanoporous membrane, is advantageous because it permits selective immune cell (or cancer cell and stem cell) transmigration through the matrix via matrix metalloproteinases (MMPs).[46]

While leukocyte migration on and through the vascular endothelial barrier is largely regulated by interactions between endothelial expressed ICAM1 and leukocyte expressed LFA1 and MAC1 integrins, the movement of these immune cells through the underlying ECM involves the combined interactions of other beta 1 integrins, MMPs, and ECM proteins.[7] In vitro studies observing the migratory patterns of leukocytes through collagen gels have allowed for the investigation of mechanisms involved in this behavior.[47–50] In order to observe the effects of a supplemented ECM on the ability to observe neutrophil migration within our mimetic, HUVECs were seeded on collagen gel-backed dual-scale membranes (1736 pores mm^{-2}) and neutrophil migration experiments were performed. The presence of the gel did not affect the ability to observe neutrophil transmigration or restrict the formation of a sufficient fMLP gradient to induce transmigration

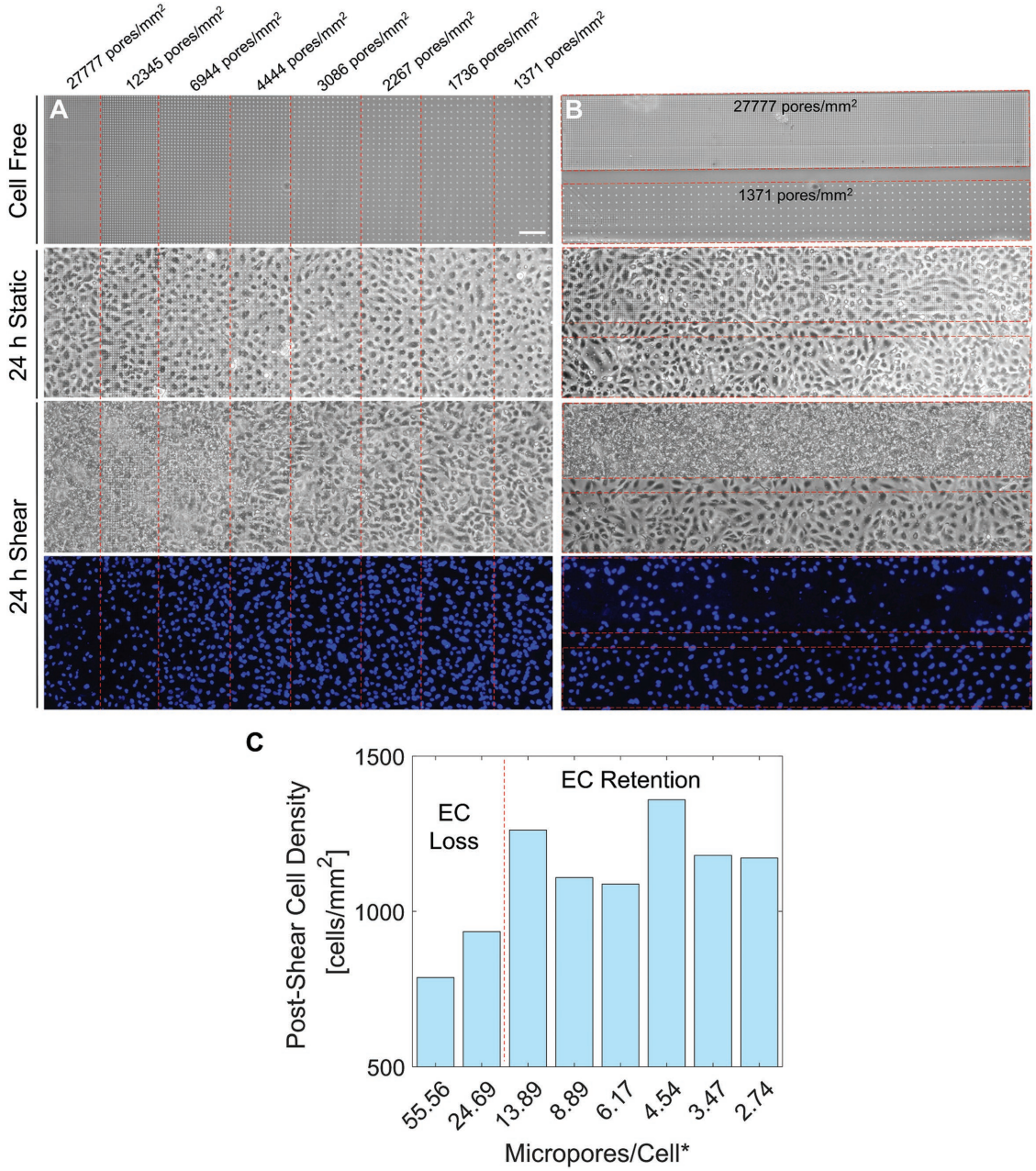

Figure 5. High micropore density leads to EC loss under fluid shear. HUVECs were seeded on A) gradient and B) side-by-side dual-scale (nano- and microporous) membranes and grown to confluency. 24 h static images represent microfluidic devices that were replenished with fresh media and returned to the incubator for an additional 24 h. 24 h shear images represent cells that were integrated into the flow circuit and sheared at 4.5 dyn cm^{-2} for an additional 24 h. Phase and fluorescent (DAPI, blue) images were recorded postflow (scale bar = 100 µm) for the same experiment. C) FIJI-assisted quantification of cell nuclei post shear. *Micropore/cell represents the number of micropores located directly underneath a given EC based on an estimated spread area of 2000 $µm^2$.

(Figure 6D). As expected, the collagen gel restricts the "fall-off" of neutrophils as they pass through the micropores. Instead, the neutrophils take on an additional step in the innate immune response cascade, in which they must crawl along and into the proteinaceous ECM. This result can be observed in Movie S5 in the Supporting Information. MMPs have also been hypothesized to influence tumor cell migration through the ECM.[51,52] Benbow and colleagues previously discovered the role of MMP-1 in the invasion of type I collagen gels by an A2058 melanoma cell line.[53] Future studies may explore the use of our gel-supplemented vascular mimetic in investigating tumor cell migration through both ECs and the supporting ECM. Overall, the addition of an underlying collagen gel both rescues cell adhesion and allows for the study of the next step in the innate immune response and tumor metastasis.

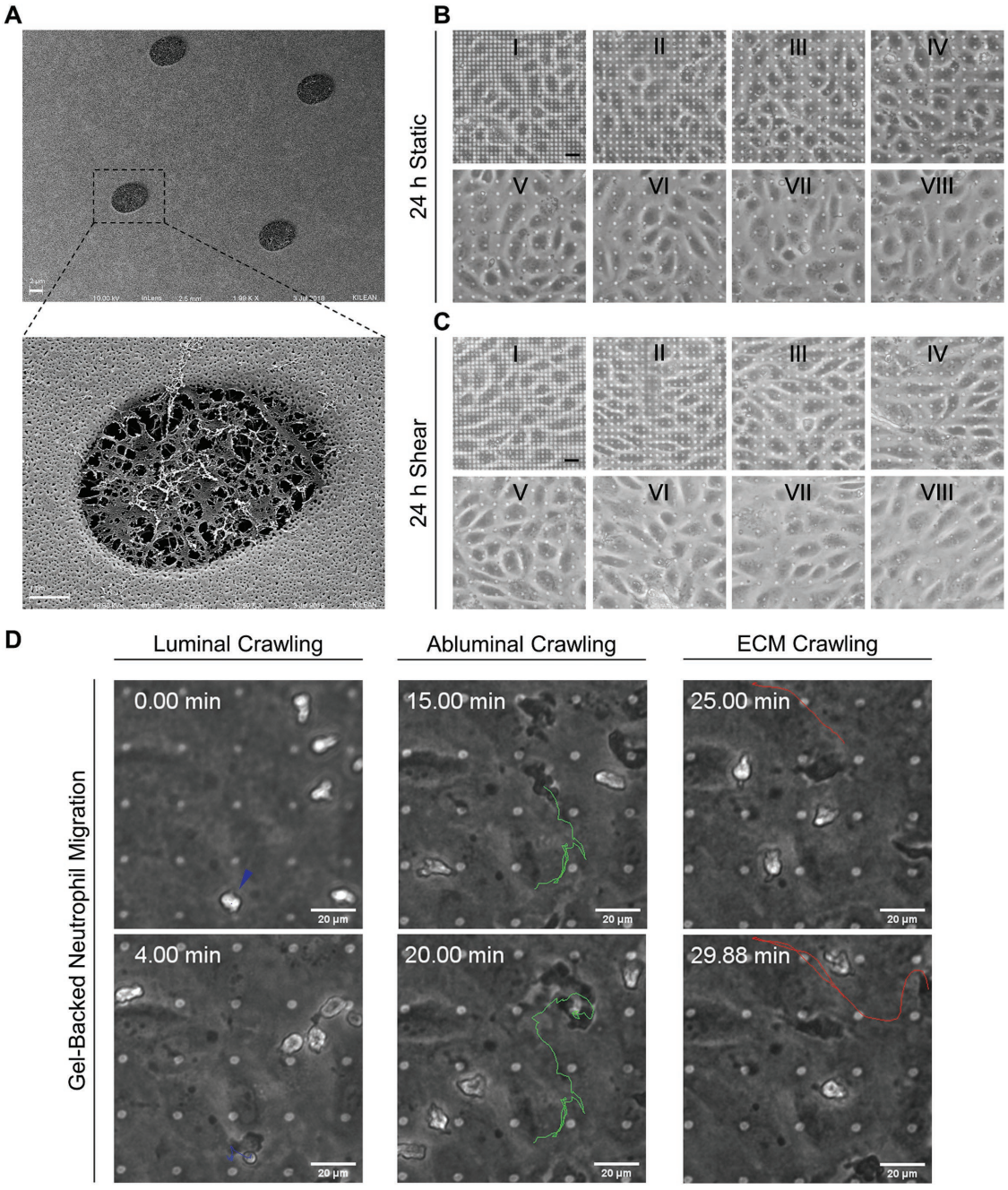

Figure 6. Submembrane collagen maintains endothelial monolayer for all micropore densities and permits leukocyte transmigration experimentation. A 300 µm collagen gel was added to the backside of a dual-scale membrane. A) SEM images were obtained of glutaraldehyde fixed samples without cells (top scale bar = 2 µm; bottom scale bar = 1 µm). B) Phase images were obtained of HUVECs seeded on collagen gel back dual-scale membranes and left to grow for 24 h after reaching confluency (scale bar = 20 µm). C) Additionally, HUVECs seeded on gel back dual-scale membranes were grown to confluency and sheared at 4.5 dyn cm^{-2} for 24 h and phase images were recorded (scale bar = 20 µm). D) Submembrane collagen gel permits neutrophil migration under an fMLP gradient, with an additional ECM crawling step. Roman numerals in panels B and C correspond to the following 3 µm pore densities (pores mm^{-2}): I = 27 777, II = 12 345, III = 6944, IV = 4444, V = 3086, VI = 2267, VII = 1736, VIII = 1371.

While it might be concluded that the use of a collagen gel may eliminate the need for a membrane all together, it must be noted that the membrane is essential for scaffolding gel polymerization and maintaining the position of the viscoelastic gel once flow begins. Furthermore, the planar membrane provides a consistent focal plane for clear phase contrast imaging even in the presence of flow pressures.

2.5. Leukocyte Transmigration Through Shear-Primed Endothelial Cell Monolayers

Shear stress is known to enhance EC barriers as shown by the direct relationship between increased transendothelial electrical resistance and prolonged shear stress.[54] This increased barrier function has been shown to also modulate neutrophil

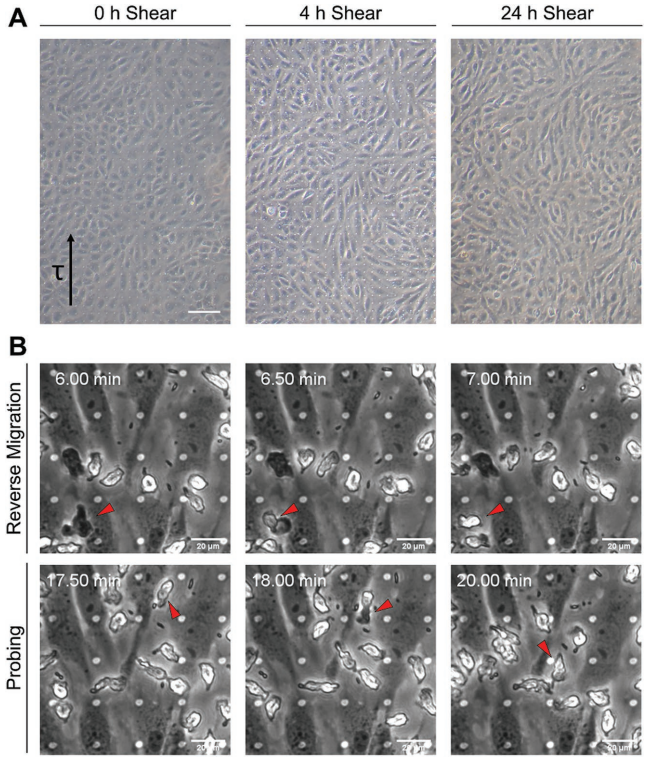

Figure 7. Dual-Scale membranes support shear priming for enhanced barrier function in leukocyte migration experimentation. A) HUVECs were seeded on dual-scale membranes (1736 pores mm^{-2}) and sheared at 4.5 dyn cm^{-2} for 24 h (scale bar = 100 µm). B) Neutrophil migration experiments were performed on the shear-primed EC monolayers. Time-lapse phase contrast imaging revealed some instances of reverse leukocyte migration and probing without complete transendothelial migration.

transmigration in response to TNFα, as demonstrated by a marked decrease in transendothelial migration events through a shear stress influenced EC monolayer.[55] With the goal of using our platform to expand on such findings, dual-scale membranes were investigated here for their ability to support long-term shear and modulate endothelial phenotype. HUVECs grown on dual-scale membranes (1736 pores mm^{-2}) were sheared at 4.5 dyn cm^{-2} for 24 h. Phase images show the EC transition from cobblestone morphology to increased elongation over the 24 h shear incubation (**Figure 7**A). Neutrophil transmigration in response to fMLP showed an observable decrease in neutrophil transmigration events, with prominent instances of reverse migration (transendothelial migration from the abluminal to luminal side) and probing without migration (Figure 7B). This result validates the ability of the dual-scale pore membranes to support shear-induced changes to vascular EC phenotype prior to the study of leukocyte migration.

3. Conclusion

We have developed a dual-scale (nano- and microporous) ultrathin membrane technology that facilitates cell transmigration studies, in a vascular model, while also providing a continuously porous substrate. This unique membrane design contains hundreds of 3 µm pores on a background of millions of closely spaced (≈100 nm) nanopores. The porosities of the membranes range from 9% to nearly 30%. Whereas existing microporous membranes may limit uniform small molecule passage due to large nonporous interpore regions, our membranes remedy this issue through the lithographic addition of micropores on a highly permeable nanoporous substrate. In the case of our vascular transmigration model, this creates a physiologically relevant presentation of chemoattractant to both the endothelium and circulating immune cells. Our rapid, iterative membrane fabrication protocol (≈2 h) allowed us to study the effects of micropore density on EC adhesion. It was determined that micropore densities larger than ≈14 per cell limit cell–substrate interaction, resulting in EC loss under shear, but that the addition of a physiologically relevant collagen gel under the micropores eliminates this loss. While the benefits of our dual-scale membranes in a vascular model setting are explored in detail here, future work will explore the use of these membranes in a varity of settings, not limited to organ-on-a-chip platforms, separations and capture kinetics, and sensor systems.

4. Experimental Section

Transfer of Micropores: NPN,[34] membranes (Figure S1A, Supporting Information) were purchased from SiMPore Inc. (Rochester, NY) with average pore size of 44.6 nm and membrane thickness equal to 100 nm. Membranes were adhered to a standard glass slide using carbon double-sided adhesive tape. Glass slides were then attached to a 20 mm spinner vacuum chuck for the resist spinning process. The use of an intermediate glass slide allowed for coating of free-standing membranes without the influence of the vacuum pulling on the nanomembrane (Figure S2, Supporting Information). To enhance resist adhesion, a P20 hexamethyldisilazane solution was spin-coated onto the nanomembrane at 7000 RPM for 50 s. Using the manufacturer protocol, Shipley 1805 positive photoresist was spun down onto the membranes to create a uniform 500 nm coating. The spin coat process was followed by a 60 s soft bake at 115 °C. Photoresist-coated membranes were patterned using a laser writer system (MICROTECH, Palermo, Italy). Membranes were loaded directly into the laser writer sample tray without modification. Using a pore pattern designed in the accompanying CleWin5 software, resist was selectively exposed to a 233 mJ cm^{-2} columnated beam and subsequently developed in Microposit MF-319. Various pore patterns and densities (1371–27 777 pores mm^{-2}) were written onto the nanoporous membranes. Patterned membranes were then etched in an RIE system (South Bay Technology Inc., San Clemente, CA). A three-gas silicon etch recipe (15 SCCM O_2, 10 SCCM CHF_3, 30 SCCM SF_6, 200 s, 30–50 mTorr, 100 W) was used to remove exposed NPN, resulting in a successful transfer of the micropore pattern into the free-standing nanoporous membrane. A subsequent oxygen plasma ash step in the RIE (55 SCCM O_2, 15 min, 200 mTorr, 100 W) was used to selectively remove the remaining photoresist, leaving a clean, dual-scale (nano- and microporous) membrane.

Microfluidic Device Fabrication: For cell culture and transmigration experiments, dual-scale membranes were integrated into a silicone based microfluidic device. Pressure sensitive adhesive (3 M, Maplewood, MN; 130 µm thick) and silicone gasket (Trelleborg, Trelleborg, Sweden; 300 µm thick) were cut to specification (Figure S1B, Supporting Information) using a Silhouette Cameo craft cutter system.[56] Layers were irreversibly bonded together following a 15 min UV–ozone exposure and 2 h thermal curing at 70 °C. The dual-scale membrane was sandwiched in between layers, creating defined luminal and abluminal channels. Polydimethylsiloxane made from a Sylgard 184 kit

was used as a pipette/tubing access layer. The assembled device (Figure S1C, Supporting Information) was bonded to a #1.5 coverslip, allowing for unobstructed optical imaging. In flow experiments, devices were connected in circuit to a media reservoir (placed postdevice), fluidic capacitor (placed predevice), and peristaltic pump (placed in between reservoir and capacitor; Figure S1D, Supporting Information). The inclusion of the air-tight fluidic capacitor (Figure S1E, Supporting Information) dampens pressure fluctuations introduced by the peristaltic pump, while also acting as a bubble trap upstream of the cell monolayer. The capacitor was designed around a 1.5 mL cryovial with modifications that include a fluid inlet, fluid outlet, and glass slide base. Media flow rate was set to achieve a cell layer shear stress equal to 4.5 dyn cm^{-2} as determined by Equation (2)

$$\tau = \frac{6Q\mu}{h^2 w} \tag{2}$$

where Q represents the input flow rate, μ is the media viscosity, h is the height of the channel directly over the cell monolayer, and w is the width of the channel.

Cell Culture: HUVECs were purchased from VEC Technologies (Rensselaer, NY; Product# HUVECP). Pooled HUVECs were selected over single source to prevent result bias due to cell population homogeneity. HUVECs were maintained in T25 flasks at 37 °C, 5% CO_2 in MCDB-131 Complete media (VEC Technologies) and used between passage numbers 3 and 7 as recommended by the supplier. Following microfluidic device assembly, silicon membranes were coated with 0.17 mg mL^{-1} human fibronectin (BD Biosciences, Franklin Lakes, NJ) for 1 h at room temperature to facilitate cell adhesion. HUVECs were trypsinized and perfused into the luminal channel at a density necessary to achieve 40 000 cells cm^{-2}. The perfusion was performed with a P20 pipette placed directly in the PDMS access layer port. Gentle introduction of the cell bolus ensured uniform cell seeding. Following perfusion, cells were allowed to adhere and grow to confluency over 24 h under standard culture conditions listed above. In experiments involving shear stress, microfluidic devices were added to the flow circuit 24 h post cell perfusion. For cell counting, 4% paraformaldehyde fixed cell nuclei were stained using a 1 µg mL^{-1} solution of 4-6-diamidino-2-phenylindole (DAPI) in 1X phosphate-buffered saline (PBS). Epifluorescence images were imported into FIJI and converted to 16-bit. The image threshold was adjusted to isolate DAPI staining. "Touching" nuclei were divided using the watershed plugin (Process > Binary > Watershed). Cell nuclei were automatically counted in regions of interest using the particle analysis feature in FIJI (Analyze > Analyze Particles). Cell counts were normalized to area of the membrane region specified in our results. Cell culture experiments were performed in triplicate.

Neutrophil Transmigration: Human neutrophils were isolated from consenting healthy donors using a previously described, IRB approved protocol.[57] Briefly, whole blood collected in sodium heparin vacuum tubes was density separated using 1-Step Polymorph (Accurate Chemical & Scientific Co., Westbury, NY). The collected neutrophil rich solution was washed and rid of red blood cells using a lysis step. The resulting neutrophil pure pellet was stored in Hank's balanced salt solution with added 10×10^{-3} M 4-(2-hydroxyethyl)-1-piperazineethanesulfonic acid and 5 mg mL^{-1} bovine serum albumin to prevent nonspecific activation prior to experimentation. Neutrophils were used within 3 h postisolation (5 h postblood draw). Immediately prior to device perfusion, neutrophils were removed from their suspension buffer and transferred to MCDB-131 complete media (VEC Technologies; HUVEC media) at a concentration equal to 6 million cells mL^{-1}. Neutrophils were then introduced to the luminal channel and allowed to settle on the HUVEC monolayer. To promote chemotaxis, 10 nM fMLP (Sigma, Darmstadt, Germany) in MCDB-131 complete media was added to the abluminal channel. The prepared device was then transferred to a modified incubation chamber (PECON, Erbach, Germany) surrounding a Nikon TS100 microscope to allow for time lapse imaging in a controlled environment. Time from introduction of fMLP to initiation of time lapse imaging was less than a minute. All transmigration videos were recorded at 40×, 4 fpm over 30 min.

Collagen Gel: A 2 mg mL^{-1} solution of type 1 rat tail collagen (Enzo Life Sciences, Farmingdale, NY) was prepared on ice. A combination of NaOH, diH_2O, and 10× PBS was used to facilitate the gelling process. While cold, the collagen solution was pipetted into the 300 µm "trench" between the bottom of the silicon supports surrounding the free-standing membrane, and the membrane itself. Membranes were placed in an incubator (37 °C, 5% CO_2) for 1 h to permit gelling. Gel-backed membranes were then used in the same fashion as the clean membranes for cell culture. A 2.5% glutaraldehyde solution was used to fix gel-backed membranes for scanning electron microscopy (SEM).

Supporting Information

Supporting Information is available from the Wiley Online Library or from the author.

Acknowledgements

The authors gratefully acknowledge B. McIntyre and J. Mitchell in supporting the use of the UR Nano clean room facilities. The authors would like to acknowledge K. Lucas for SEM work, R. Breidenstein for microfluidic device fabrication, and B. Kwarta and J. Cox for their illustrations. Research reported in this publication was supported in part by NIGMS of the National Institute of Health (NIH) under award number R35GM119623 (T.G.). The cell culture work was supported by the US Public Health Service through the NIH under award number R01 HL125265 (R.W. and J.L.M.). A.S. is currently supported under NIH training grant 2T32 HL066988-16A1. The content of this publication is solely the responsibility of the authors and does not necessarily represent the official views of the NIH.

Conflict of Interest

The authors declare the following competing financial interest(s): J.L.M. and T.R.G. are co-founders of SiMPore, an early-stage company commercializing ultrathin silicon-based technologies.

Keywords

dual-scale, nanoporous silicon nitride, shear stress, transmigration, vascular mimetic

Received: October 5, 2018
Revised: November 26, 2018
Published online:

[1] S. Nourshargh, R. Alon, *Immunity* **2014**, *41*, 694.
[2] S. M. Hamilla, K. M. Stroka, H. Aranda-Espinoza, *PLoS One* **2014**, *9*, e109748.
[3] G. S. L. Teo, J. A. Ankrum, R. Martinelli, S. E. Boetto, K. Simms, T. E. Sciuto, A. M. Dvorak, J. M. Karp, C. V. Carman, *Stem Cells* **2012**, *30*, 2472.
[4] G. S. L. Teo, Z. Yang, C. V. Carman, J. M. Karp, C. P. Lin, *Stem Cells* **2015**, *33*, 265.
[5] W. Weninger, M. Biro, R. Jain, *Nat. Rev. Immunol.* **2014**, *14*, 232.
[6] D. Vestweber, *Nat. Rev. Immunol.* **2015**, *15*, 692.
[7] K. Ley, C. Laudanna, M. I. Cybulsky, S. Nourshargh, *Nat. Rev. Immunol.* **2007**, *7*, 678.

[8] M. D. Cahalan, I. Parker, S. H. Wei, M. J. Miller, *Nat. Rev. Immunol.* **2002**, *2*, 872.
[9] S. H. Baik, M.-Y. Cha, Y.-M. Hyun, H. Cho, B. Hamza, D. K. Kim, S.-H. Han, H. Choi, K. H. Kim, M. Moon, J. Lee, M. Kim, D. Irimia, I. Mook-Jung, *Neurobiol. Aging* **2014**, *35*, 1286.
[10] M. I. Bogorad, J. DeStefano, J. Karlsson, A. D. Wong, S. Gerecht, P. C. Searson, *Lab Chip* **2015**, *15*, 4242.
[11] H. H. Chung, M. Mireles, B. J. Kwarta, T. R. Gaborski, *Lab Chip* **2018**, *18*, 1671.
[12] J. A. Brown, V. Pensabene, D. A. Markov, V. Allwardt, M. D. Neely, M. Shi, C. M. Britt, O. S. Hoilett, Q. Yang, B. M. Brewer, P. C. Samson, L. J. McCawley, J. M. May, D. J. Webb, D. Li, A. B. Bowman, R. S. Reiserer, J. P. Wikswo, *Biomicrofluidics* **2015**, *9*, 054124.
[13] S. H. Ma, L. A. Lepak, R. J. Hussain, W. Shain, M. L. Shuler, *Lab Chip* **2005**, *5*, 74.
[14] B. M. Maoz, A. Herland, E. A. FitzGerald, T. Grevesse, C. Vidoudez, A. R. Pacheco, S. P. Sheehy, T. E. Park, S. Dauth, R. Mannix, N. Budnik, K. Shores, A. Cho, J. C. Nawroth, D. Segre, B. Budnik, D. E. Ingber, K. K. Parker, *Nat. Biotechnol.* **2018**, *36*, 865.
[15] F. Kukulski, F. Ben Yebdri, J. Lefebvre, M. Warny, P. A. Tessier, J. Sevigny, *J. Leukocyte Biol.* **2007**, *81*, 1269.
[16] A. Albini, Y. Iwamoto, H. K. Kleinman, G. R. Martin, S. A. Aaronson, J. M. Kozlowski, R. N. McEwan, *Cancer Res.* **1987**, *47*, 3239.
[17] R. N. Carter, S. M. Casillo, A. R. Mazzocchi, J. S. DesOrmeaux, J. A. Roussie, T. R. Gaborski, *Biofabrication* **2017**, *9*, 015019.
[18] A. R. Mazzocchi, A. J. Man, J.-P. S. DesOrmeaux, T. R. Gaborski, *Cell Mol. Bioeng.* **2014**, *7*, 369.
[19] T. Pasman, D. Grijpma, D. Stamatialis, A. Poot, *J. R. Soc., Interface* **2018**, *15*, 20180351.
[20] D. Huh, B. D. Matthews, A. Mammoto, M. Montoya-Zavala, H. Y. Hsin, D. E. Ingber, *Science* **2010**, *328*, 1662.
[21] D. Huh, D. C. Leslie, B. D. Matthews, J. P. Fraser, S. Jurek, G. A. Hamilton, K. S. Thorneloe, M. A. McAlexander, D. E. Ingber, *Sci. Transl. Med.* **2012**, *4*, 159ra147.
[22] S. M. Casillo, A. P. Peredo, S. J. Perry, H. H. Chung, T. R. Gaborski, *ACS Biomater. Sci. Eng.* **2017**, *3*, 243.
[23] A. Mossu, M. Rosito, T. Khire, H. L. Chung, H. Nishihara, I. Gruber, E. Luke, L. Dehouck, F. Sallusto, F. Gosselet, J. McGrath, B. Engelhardt, *J. Cereb. Blood Flow Metab.* **2018**, *0*, 1.
[24] F. Zheng, F. Fu, Y. Cheng, C. Wang, Y. Zhao, Z. Gu, *Small* **2016**, *12*, 2253.
[25] S. Santaguida, D. Janigro, M. Hossain, E. Oby, E. Rapp, L. Cucullo, *Brain Res.* **2006**, *1109*, 1.
[26] R. Booth, H. Kim, *Lab Chip* **2012**, *12*, 1784.
[27] A. A. Agrawal, B. J. Nehilla, K. V. Reisig, T. R. Gaborski, D. Z. Fang, C. C. Striemer, P. M. Fauchet, J. L. McGrath, *Biomaterials* **2010**, *31*, 5408.
[28] B. J. Nehilla, N. Nataraj, T. R. Gaborski, J. L. McGrath, *Acta Biomater.* **2014**, *10*, 4670.
[29] T. S. Khire, B. J. Nehilla, J. Getpreecharsawas, M. E. Gracheva, R. E. Waugh, J. L. McGrath, *Biomed. Microdevices* **2018**, *20*, 11.
[30] C. C. Striemer, T. R. Gaborski, J. L. McGrath, P. M. Fauchet, *Nature* **2007**, *445*, 749.
[31] T. R. Gaborski, J. L. Snyder, C. C. Striemer, D. Z. Fang, M. Hoffman, P. M. Fauchet, J. L. McGrath, *ACS Nano* **2010**, *4*, 6973.
[32] D. G. Johnson, T. S. Khire, Y. L. Lyubarskaya, K. J. Smith, J. P. Desormeaux, J. G. Taylor, T. R. Gaborski, A. A. Shestopalov, C. C. Striemer, J. L. McGrath, *Adv. Chronic Kidney Dis.* **2013**, *20*, 508.
[33] K. Y. Morgan, D. Sklaviadis, Z. L. Tochka, K. M. Fischer, K. Hearon, T. D. Morgan, R. Langer, L. E. Freed, *Adv. Funct. Mater.* **2016**, *26*, 5873.
[34] J. P. DesOrmeaux, J. D. Winans, S. E. Wayson, T. R. Gaborski, T. S. Khire, C. C. Striemer, J. L. McGrath, *Nanoscale* **2014**, *6*, 10798.
[35] L. C. Kelley, L. L. Lohmer, E. J. Hagedorn, D. R. Sherwood, *J. Cell Biol.* **2014**, *204*, 291.
[36] R. G. Rowe, S. J. Weiss, *Trends Cell Biol.* **2008**, *18*, 560.
[37] R. Ishimatsu, J. Kim, P. Jing, C. C. Striemer, D. Z. Fang, P. M. Fauchet, J. L. McGrath, S. Amemiya, *Anal. Chem.* **2010**, *82*, 7127.
[38] A. Marino, O. Tricinci, M. Battaglini, C. Filippeschi, V. Mattoli, E. Sinibaldi, G. Ciofani, *Small* **2018**, *14*, 1702959.
[39] L. S. Worrel, J. A. Morehouse, L. A. Shimko, D. R. Lloyd, D. F. Lawler, B. D. Freeman, *Sep. Purif. Technol.* **2007**, *53*, 71.
[40] L. Sorokin, *Nat. Rev. Immunol.* **2010**, *10*, 712.
[41] H. M. Lauridsen, J. S. Pober, A. L. Gonzalez, *FASEB J.* **2014**, *28*, 1166.
[42] W. A. Muller, F. W. Luscinskas, *Methods Enzymol.* **2008**, *443*, 155.
[43] K. M. Gray, K. M. Stroka, *Semin. Cell Dev. Biol.* **2017**, *71*, 106.
[44] G. Cinamon, V. Shinder, R. Alon, *Nat. Immunol.* **2001**, *2*, 515.
[45] W. C. Aird, *J. Thromb. Haemostasis* **2005**, *3*, 1392.
[46] S. A. Siefert, R. Sarkar, *Vascular* **2012**, *20*, 210.
[47] A. M. Tester, J. H. Cox, A. R. Connor, A. E. Starr, R. A. Dean, X. S. Puente, C. Lopez-Otin, C. M. Overall, *PLoS One* **2007**, *2*, e312.
[48] M. Lin, P. Jackson, A. M. Tester, E. Diaconu, C. M. Overall, J. E. Blalock, E. Pearlman, *Am. J. Pathol.* **2008**, *173*, 144.
[49] M. R. Parkhurst, W. M. Saltzman, *Biophys. J.* **1992**, *61*, 306.
[50] P. C. Wilkinson, *J. Immunol. Methods* **1998**, *216*, 139.
[51] Shuman Moss, L. A. , S. Jensen-Taubman, W. G. Stetler-Stevenson, *Am. J. Pathol.* **2012**, *181*, 1895.
[52] K. Hotary, E. Allen, A. Punturieri, I. Yana, S. J. Weiss, *J. Cell Biol.* **2000**, *149*, 1309.
[53] U. Benbow, M. P. Schoenermark, T. I. Mitchell, J. L. Rutter, K. Shimokawa, H. Nagase, C. E. Brinckerhoff, *J. Biol. Chem.* **1999**, *274*, 25371.
[54] J. Seebach, P. Dieterich, F. Luo, H. Schillers, D. Vestweber, H. Oberleithner, H.-J. Galla, H.-J. Schnittler, *Lab. Invest.* **2000**, *80*, 1819.
[55] S. Sheikh, G. E. Rainger, Z. Gale, M. Rahman, G. B. Nash, *Blood* **2003**, *102*, 2828.
[56] P. K. Yuen, V. N. Goral, *Lab Chip* **2010**, *10*, 384.
[57] H. H. Chung, C. K. Chan, T. S. Khire, G. A. Marsh, A. Clark Jr., R. E. Waugh, J. L. McGrath, *Lab Chip* **2014**, *14*, 2456.